Title

The Backup Program of the Dark Energy Spectroscopic Instrument's Milky Way Survey

Journal

The Astronomical Journal, 171(6)

ISSN

0004-6256

Authors

Dey, Arjun
Koposov, Sergey E
Najita, Joan R
et al.

Publication Date

2026-06-01

DOI

10.3847/1538-3881/ae5dd0

The Astronomical Journal, 171:348 (16pp), 2026 June https://doi.org/10.3847/1538-3881/ae5dd0

The Backup Program of the Dark Energy Spectroscopic Instrument's Milky Way Survey

Arjun Dey[1], Sergey E. Koposov[2,3], Joan R. Najita[1], Andrew P. Cooper[4,5], B. T. Gänsicke[6], Adam D. Myers[7], A. Raichoor[8], Daniel J. Eisenstein[9], E. F. Schlafly[10], D. Schlegel[8], C. Allende Prieto[11], Leandro Beraldo e Silva[12,13], Ting S. Li[14], M. Valluri[15], Stéphanie Juneau[1], Mika Lambert[16], S. Li[17,18,19], Guillaume F. Thomas[20,21], Wenting Wang[22], Alexander H. Riley[23], N. Kizhuprakkat[4,5], J. Aguilar[8], S. Ahlen[24], S. Bailey[8], D. Bianchi[25,26], D. Brooks[27], T. Claybaugh[8], A. Cuceu[8], A. de la Macorra[28], J. Della Costa[29,1], Biprateep Dey[30,31], P. Doel[27], A. Font-Ribera[32], J. E. Forero-Romero[33,34], E. Gaztañaga[35,36,37], S. Gontcho A Gontcho[8], G. Gutierrez[38], J. Guy[8], C. Hahn[39], K. Honscheid[40,41,42], M. Ishak[43], J. Jimenez[32], R. Kehoe[44], D. Kirkby[45], T. Kisner[8], A. Kremin[8], C. Lamman[9], M. Landriau[8], L. Le Guillou[46], M. E. Levi[8], M. Manera[32,47], P. Martini[40,42,48], A. Meisner[1], R. Miquel[32,49], J. Moustakas[50], S. Nadathur[36], N. Palanque-Delabrouille[8,51], W. J. Percival[52,53,54], I. Pérez-Ràfols[56], F. Prada[55], G. Rossi[57], E. Sanchez[58], M. Schubnell[59,60], J. Silber[8], D. Sprayberry[1], G. Tarlé[60], B. A. Weaver[1], R. H. Wechsler[61,62,63], R. Zhou[8], and H. Zou[64]

[1] NSF NOIRLab, 950 North Cherry Avenue, Tucson, AZ 85719, USA; arjun.dey@noirlab.edu
[2] Institute for Astronomy, University of Edinburgh, Royal Observatory, Blackford Hill, Edinburgh EH9 3HJ, UK
[3] Institute of Astronomy, University of Cambridge, Madingley Road, Cambridge CB3 0HA, UK
[4] Institute of Astronomy and Department of Physics, National Tsing Hua University, Hsinchu 30013, Taiwan
[5] Center for Informatics and Computation in Astronomy, National Tsing Hua University, Hsinchu 30013, Taiwan
[6] Department of Physics, University of Warwick, Coventry, CV4 7AL, UK
[7] Department of Physics and Astronomy, University of Wyoming, Laramie, WY 82071, USA
[8] Lawrence Berkeley National Laboratory, 1 Cyclotron Road, Berkeley, CA 94720, USA
[9] Center for Astrophysics | Harvard & Smithsonian, 60 Garden Street, Cambridge, MA 02138, USA
[10] Space Telescope Science Institute, 3700 San Martin Drive, Baltimore, MD 21218, USA
[11] Instituto de Astrofísica de Canarias, C/ Vía Láctea, s/n, 38205, San Cristóbal de La Laguna, Santa Cruz de Tenerife, Spain
[12] Steward Observatory and Department of Astronomy, University of Arizona, 933 North Cherry Avenue, Tucson, AZ 85721, USA
[13] Observatório Nacional, Rio de Janeiro—RJ, 20921-400, Brasil
[14] Department of Astronomy and Astrophysics, University of Toronto, 50 Saint George Street, Toronto ON, M5S 3H4, Canada
[15] Department of Astronomy, University of Michigan, Ann Arbor, MI 48109, USA
[16] Department of Astronomy & Astrophysics, University of California, Santa Cruz, 1156 High Street, Santa Cruz, CA 95064, USA
[17] Department of Astronomy, School of Physics and Astronomy, Shanghai Jiao Tong University, Shanghai 200240, People's Republic of China
[18] Shanghai Key Laboratory for Particle Physics and Cosmology, Shanghai 200240, People's Republic of China
[19] State Key Laboratory of Dark Matter Physics, School of Physics and Astronomy, Shanghai Jiao Tong University, Shanghai 200240, People's Republic of China
[20] Instituto de Astrofísica de Canarias, E-38205 La Laguna, Tenerife, Spain
[21] Universidad de La Laguna, Departamento Astrofísica, E-38206 La Laguna, Tenerife, Spain
[22] Department of Astronomy, School of Physics and Astronomy, and Shanghai Key Laboratory for Particle Physics and Cosmology, Shanghai Jiao Tong University, Shanghai 200240, People's Republic of China
[23] Institute for Computational Cosmology, Department of Physics, Durham University, South Road, Durham DH1 3LE, UK
[24] Department of Physics, Boston University, 590 Commonwealth Avenue, Boston, MA 02215, USA
[25] Dipartimento di Fisica "Aldo Pontremoli," Università degli Studi di Milano, Via Celoria 16, I-20133 Milano, Italy
[26] INAF—Osservatorio Astronomico di Brera, Via Brera 28, 20122 Milano, Italy
[27] Department of Physics & Astronomy, University College London, Gower Street, London, WC1E 6BT, UK
[28] Instituto de Física, Universidad Nacional Autónoma de México, Circuito de la Investigación Científica, Ciudad Universitaria, Ciudad de México C. P. 04510, México
[29] Department of Astronomy, San Diego State University, 5500 Campanile Drive, San Diego, CA 92182, USA
[30] Department of Astronomy & Astrophysics, University of Toronto, Toronto, ON M5S 3H4, Canada
[31] Department of Physics & Astronomy and Pittsburgh Particle Physics, Astrophysics, and Cosmology Center (PITT PACC), University of Pittsburgh, 3941 O'Hara Street, Pittsburgh, PA 15260, USA
[32] Institut de Física d'Altes Energies (IFAE), The Barcelona Institute of Science and Technology, Edifici Cn, Campus UAB, 08193, Bellaterra (Barcelona), Spain
[33] Departamento de Física, Universidad de los Andes, Carrera 1 No. 18A-10, Edificio Ip, CP 111711, Bogotá, Colombia
[34] Observatorio Astronómico, Universidad de los Andes, Carrera 1 No. 18A-10, Edificio H, CP 111711 Bogotá, Colombia
[35] Institut d'Estudis Espacials de Catalunya (IEEC), c/ Esteve Terradas 1, Edifici RDIT, Campus PMT-UPC, 08860 Castelldefels, Spain
[36] Institute of Cosmology and Gravitation, University of Portsmouth, Dennis Sciama Building, Portsmouth, PO1 3FX, UK
[37] Institute of Space Sciences, ICE-CSIC, Campus UAB, Carrer de Can Magrans s/n, 08913, Bellaterra, Barcelona, Spain
[38] Fermi National Accelerator Laboratory, PO Box 500, Batavia, IL 60510, USA
[39] Steward Observatory, University of Arizona, 933 North Cherry Avenue, Tucson, AZ 85721, USA
[40] Center for Cosmology and AstroParticle Physics, The Ohio State University, 191 West Woodruff Avenue, Columbus, OH 43210, USA
[41] Department of Physics, The Ohio State University, 191 West Woodruff Avenue, Columbus, OH 43210, USA
[42] The Ohio State University, Columbus, 43210 OH, USA
[43] Department of Physics, The University of Texas at Dallas, 800 West Campbell Road, Richardson, TX 75080, USA
[44] Department of Physics, Southern Methodist University, 3215 Daniel Avenue, Dallas, TX 75275, USA
[45] Department of Physics and Astronomy, University of California, Irvine, 92697, USA
[46] Sorbonne Université, CNRS/IN2P3, Laboratoire de Physique Nucléaire et de Hautes Energies (LPNHE), FR-75005 Paris, France
[47] Departament de Física, Serra Húnter, Universitat Autònoma de Barcelona, 08193, Bellaterra (Barcelona), Spain
[48] Department of Astronomy, The Ohio State University, 4055 McPherson Laboratory, 140 West 18th Avenue, Columbus, OH 43210, USA
[49] Institució Catalana de Recerca i Estudis Avançats, Passeig de Lluís Companys, 23, 08010 Barcelona, Spain
[50] Department of Physics and Astronomy, Siena College, 515 Loudon Road, Loudonville, NY 12211, USA
[51] IRFU, CEA, Université Paris-Saclay, F-91191 Gif-sur-Yvette, France
[52] Department of Physics and Astronomy, University of Waterloo, 200 University Avenue West, Waterloo, ON N2L 3G1, Canada

[53] Perimeter Institute for Theoretical Physics, 31 Caroline Street North, Waterloo, ON N2L 2Y5, Canada
[54] Waterloo Centre for Astrophysics, University of Waterloo, 200 University Avenue West, Waterloo, ON N2L 3G1, Canada
[55] Instituto de Astrofísica de Andalucía (CSIC), Glorieta de la Astronomía, s/n, E-18008 Granada, Spain
[56] Departament de Física, EEBE, Universitat Politècnica de Catalunya, c/Eduard Maristany 10, 08930 Barcelona, Spain
[57] Department of Physics and Astronomy, Sejong University, 209 Neungdong-ro, Gwangjin-gu, Seoul 05006, Republic of Korea
[58] CIEMAT, Avenida Complutense 40, E-28040 Madrid, Spain
[59] Department of Physics, University of Michigan, 450 Church Street, Ann Arbor, MI 48109, USA
[60] University of Michigan, 500 South State Street, Ann Arbor, MI 48109, USA
[61] Kavli Institute for Particle Astrophysics and Cosmology, Stanford University, Menlo Park, CA 94305, USA
[62] Physics Department, Stanford University, Stanford, CA 93405, USA
[63] SLAC National Accelerator Laboratory, 2575 Sand Hill Road, Menlo Park, CA 94025, USA
[64] National Astronomical Observatories, Chinese Academy of Sciences, A20 Datun Road, Chaoyang District, Beijing, 100101, People's Republic of China
Received 2025 May 22; revised 2026 March 23; accepted 2026 March 26; published 2026 May 13

Abstract

The Milky Way Backup Program (MWBP), a survey currently underway with the Dark Energy Spectroscopic Instrument (DESI) on the Nicholas U. Mayall 4 m Telescope, works at the margins of the DESI Main surveys to obtain spectra of millions of additional stars from the Gaia catalog. Efficiently utilizing times between $\sim 12^\circ$ and 18° twilight and poor weather conditions, the MWBP extends the range of stellar sources studied to both brighter magnitudes and lower Galactic latitude and declination than the stars studied in DESI's Main Milky Way Survey. While the MWBP prioritizes candidate giant stars selected from the Gaia catalog (using color and parallax criteria), it also includes an unbiased sample of bright stars (i.e., $11.2 \lesssim G < 16$ mag) as well as fainter sources (to $G \lesssim 19$ mag). As of 2025 March 1, the survey had obtained spectra of $\sim$7 million stars, approximately 1.2 million of which are included in the DESI Data Release 1. The DESI spectra cover the wavelength range from 3600 to 9800 Å at a resolution $\lambda/\Delta\lambda$ varying from 2000 to 5000. The full survey, when completed, will cover an area of more than 21,000 deg^2 and include approximately 10 million Gaia sources, roughly equal to the number of stellar spectra obtained through the DESI Main Survey, while only utilizing $\approx$9% of all DESI observing time. This paper provides an overview of the MWBP, describing the target selection, observing strategy, and an introduction to the resulting data.

Unified Astronomy Thesaurus concepts: Sky surveys (1464); Redshift surveys (1378); Galaxy stellar content (621); Stellar kinematics (1608); Milky Way Galaxy (1054); Giant stars (655)

1. Introduction

The Dark Energy Spectroscopic Instrument (DESI; DESI Collaboration et al. 2022, 2016) on the Nicholas U. Mayall 4 m Telescope of the Kitt Peak National Observatory is undertaking a 5 yr mission with the primary goal of measuring the cosmological parameters that define the accelerating expansion history of the Universe (e.g., DESI Collaboration et al. 2025a, 2025b, 2025c, 2025d; A. G. Adame et al. 2025). The major portion of the cosmological survey is carried out during dark time, when the contribution of moonlight to the sky background is minimal and redshifts of faint, distant galaxies can be measured with high precision (E. F. Schlafly et al. 2023). During bright time, the project targets a nearby bright galaxy sample (C. Hahn et al. 2023) and, in addition, measures the radial velocities of millions of stars in the Milky Way (MW). While this latter bright-time survey (the Main Milky Way Survey, hereinafter MWS) is primarily aimed at measuring the kinematics of the stellar halo of the MW, it will also yield stellar parameters ($T_{\rm eff}$, $\log g$, [Fe/H], [α/Fe], and some elemental abundances) for several million stars (A. P. Cooper et al. 2023).

These dark-time and bright-time surveys (which we refer to here as the DESI Main Survey) occupy all the "good" observing conditions, when the sky is mostly clear and the sky brightness permits these primary survey observations to be carried out efficiently. However, for a significant fraction of time, the conditions are too poor to carry out the main program, but the dome can remain open and the telescope and instrument are usable for observations. These conditions can occur during morning or evening twilights (i.e., typically when the Sun is between $\sim 12^\circ$ and 18° below the horizon); at times when there is no threat of rain, but the sky is very cloudy or changeable; or when the combination of moonlight and thin clouds makes the sky brightness too high to carry out the Main Survey. But even these "worst of times" can result in scientifically productive data. During these periods, we carry out the Milky Way Survey Backup Program (MWBP). The MWBP works on the margins of the DESI Main survey: the DESI observing team tracks the weather conditions and determines when to switch to the MWBP and when the Main Survey observations can recommence.

In making efficient use of poor weather conditions, the MWBP complements the MWS and significantly increases the total number of stellar targets observed. First, the MWBP covers a larger footprint than the MWS, extending to lower Galactic latitude. Second, the MWBP extends to brighter stellar targets. Third, the MWBP sparsely samples fainter stars, down to Gaia magnitudes of $G \simeq 19$ mag. These measurements are motivated by the desire to significantly increase (beyond the DESI Main Survey) the number of tracers available for understanding the star formation history, dynamics, and assembly history of the MW's stellar components (e.g., A. P. Cooper et al. 2023), and to increase the density of probes that sample the dusty and gaseous components of the MW's interstellar medium (e.g., D. P. Finkbeiner 2003; E. F. Schlafly & D. P. Finkbeiner 2011; G. M. Green et al. 2019; A. K. Saydjari et al. 2023). Because the observations are taken under poor conditions, the spectra tend to be of lower quality than the MWS observations of similar

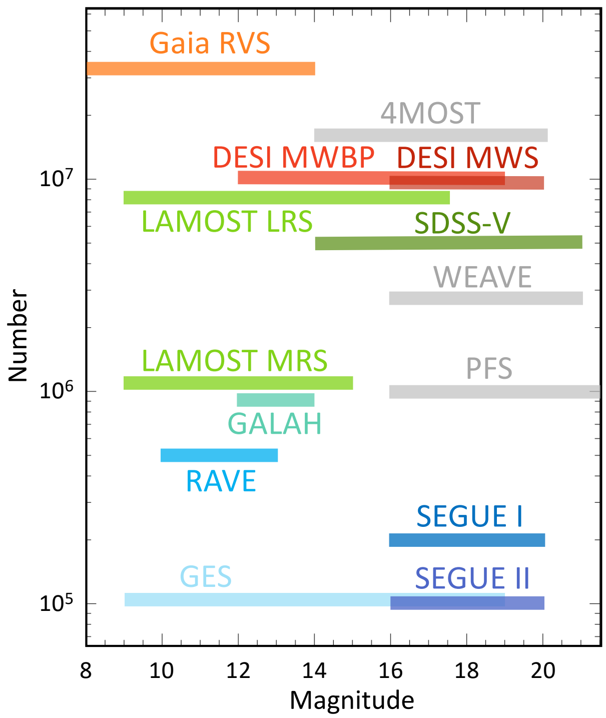

Figure 1. Comparison of the magnitude range and size of recent, ongoing (colored bars), and future (gray bars) stellar spectroscopic surveys with those of the MWBP, which is among the largest stellar spectroscopic surveys currently underway or planned. The MWBP complements the MWS in extending to brighter stars. Both surveys measure spectra for stars fainter than the Gaia Radial Velocity Spectrometer limit and are each likely to include ∼10 million stellar spectra when complete. See text for details.

magnitude stars. Nevertheless, spectra from the DESI MWBP constitute ≈22% of the stellar spectra in the DESI Data Release 1 (DESI Collaboration et al. 2026), and up to a third of the stars in the future second data release (see Section 5.2 for further details).

As of 2025 March 1, ≈9% of the available observing time has been used for the backup program, producing approximately 7 million stellar spectra. We expect that the MWBP will eventually deliver ∼10 million stellar spectra, a dataset comparable in size to the MWS and among the largest stellar spectroscopic datasets to date. Figure 1 compares the anticipated size and magnitude range of the MWBP to those of other recent (and future) spectroscopic surveys of $>10^5$ stars carried out with spectral resolution comparable to or greater than that of DESI. The parameters for the other surveys are taken from Table 1 of A. P. Cooper et al. (2023) with two exceptions and several additions. First, the number of stars in LAMOST LRS is updated with values from its DR10 v2.0 (released 2024 September 29; https://www.lamost.org/lmusers/), which includes derived stellar parameters for 7.4 million AFGK stars and 0.9 million M-type giants, dwarfs, and subdwarfs (L.-C. Deng et al. 2012; G. Zhao et al. 2012). In addition, the magnitude range for RAVE (M. Steinmetz et al. 2006, 2020a, 2020b), is converted to Gaia G-band magnitudes. Second, approximate parameters are shown for SDSS-V (A. Almeida et al. 2023), the GALAH survey (S. Buder et al. 2025),[65] the Gaia ESO Survey (GES; S. Randich et al. 2022), and the future surveys 4MOST (C. Chiappini et al. 2019),[66] WEAVE (S. Jin et al. 2024), and PFS (M. Takada et al. 2014). The relevant magnitude range is in the Gaia G band for SDSS-V, 4MOST, and WEAVE, and the V band for PSF.

In this paper, we describe the MWBP in detail to help users understand the properties of these data and the differences from the MWS. We describe the MWBP Survey target selection (Section 2), the tiling strategy (Section 3), the observational strategy (Section 4), and the data quality (Section 5), illustrating the latter with some examples. We summarize the current state of the survey in Section 6. Finally, we present a short Appendix which describes the nomenclature associated with the different DESI Stellar Surveys.

2. Target Sample Definition

The targeting pipeline for all DESI targets is described in detail by A. D. Myers et al. (2023). The primary targets for the MWBP are bright stars selected from the Gaia Data Release 2 (DR2) catalog (Gaia Collaboration et al. 2016, 2018b) across a larger footprint than the MWS (see Section 4.1.4 of A. D. Myers et al. 2023, for details). The MWBP sample is divided into five mutually exclusive classes of candidates (see Table 1 for details): bright stars with $G < 16$ mag (BACKUP_BRIGHT); candidate halo giants with $16 < G \lesssim 19$ mag, divided into high and low priority targets based on parallax error (BACKUP_GIANT and BACKUP_GIANT_LOP); and two filler samples of fainter backup stars (BACKUP_FAINT which contains stars $16 \leqslant G < 18$ mag and BACKUP_VERY_FAINT which extends this by an additional magnitude $18 \leqslant G < 19$). Targets for all classes were selected to be north of decl. $\delta = -30°$ to be accessible from the Mayall Telescope, with Gaia G, BP, and RP all fainter than ≈11.2 mag to avoid the possibility of saturating the DESI spectrum. The saturation limit as a function of $BP - RP$ color was determined from the DESI observations obtained during the survey validation phase (E. F. Schlafly et al. 2023; DESI Collaboration et al. 2024). The magnitude distribution of the MWBP stars is complementary to that of the MWS, as shown in Figure 2.

The $G < 16$ mag BACKUP_BRIGHT candidate sample contains about 46 million stars with excellent astrometric data from the Gaia satellite. Among targets with $G \geqslant 16$ mag, priority is given to candidate halo giant stars, selected based on their Gaia parallax $\pi_{\rm Gaia}$ and parallax uncertainty σ_π. The BACKUP_GIANT sample varies from about 80 stars per square degree at the North Galactic Pole (NGP) to about 220 stars per square degree at $|b| = 30°$. The MWBP subsamples the lower Galactic latitude BACKUP_GIANT sources at the rate of Min($10^{(2-\gamma)}$, 1), where

$$\gamma = \log_{10}\rho_0 \text{ if } \log_{10}\rho_0 < 0 \quad (1)$$

$$\gamma = 1.1\log_{10}\rho_0 \text{ if } \log_{10}\rho_0 > 0 \quad (2)$$

and where

$$\log_{10}\rho_0 = 6.9529434 + 0.18786695\cos(l) - 2.6621607 \times \log_{10}[|b| - 3.05095354\cos(l) + 8.10060927] \quad (3)$$

is an approximation to the variation of stellar density with Galactic longitude (l) and latitude (b) (ρ_0 in units of stars per square degree). Sources excluded by this subsampling are added to the BACKUP_GIANT_LOP candidate class. Finally, the BACKUP_FAINT and BACKUP_VERY_FAINT target samples contain a large set of fainter stars in a region that

[65] See also www.galah-survey.org/details/observing/.
[66] See also www.4most.eu/cms/science/gasconsurv.

Table 1
Selection Criteria for the Five Target Classes of the MWBP

Selection	Criteria
Cuts shared by all of the BACKUP classes:	
Sky coverage	$\delta \geqslant -30°$
Finite color	(BP − RP) ≠ *NaN*
Bright limit to avoid saturation	$G \geqslant 11.2$ mag
	BP ⩾ 11.2 mag AND RP ⩾ 11.2 mag
Primary sample (BACKUP_BRIGHT):	
Faint limit	$G < 16.0$ mag
Bright limit	$G \geqslant 11.2 + 0.6(\mathrm{BP} - \mathrm{RP})$
Galactic latitude limit	$\lvert b \rvert > 7$
High priority halo giant sample (BACKUP_GIANT):	
Faint limit	$G < \min(17.5 + 0.6(\mathrm{BP} - \mathrm{RP}), 19)$
Bright limit	$G \geqslant 16.0$ mag
Parallax	$\pi_{\mathrm{Gaia}} < 0.1$ mas $+ 2\sigma(\pi_{\mathrm{Gaia}})$
Galactic latitude limit	$\lvert b \rvert > 7$
Low priority halo giant sample (BACKUP_GIANT_LOP):	
Faint limit	$G < \min(17.5 + 0.6(\mathrm{BP} - \mathrm{RP}), 19)$
Bright limit	$G \geqslant 16.0$ mag
Parallax	$\pi_{\mathrm{Gaia}} < 0.1$ mas $+ 3\sigma(\pi_{\mathrm{Gaia}})$
Not in BACKUP_GIANT	
Galactic latitude limit	$\lvert b \rvert > 7$
Filler sample (BACKUP_FAINT):	
Faint limit	$G < 18.0$ mag
Bright limit	$G \geqslant 16.0$ mag
Not in BACKUP_GIANT	
Not in BACKUP_GIANT_LOP	
Exclude Galactic plane	(($b > -0.139\,l + 25°$ AND $l \leqslant 180°$)
	OR ($b > 0.139\,l - 25°$ AND $l > 180°$)
	OR ($b < -0.139\,l + 25°$ AND $l > 180°$)
	OR ($b < 0.139\,l - 25°$ AND $l \leqslant 180°$))
Filler sample (BACKUP_VERY_FAINT):	
Faint limit	$G < 19.0$ mag
Bright limit	$G \geqslant 18.0$ mag
Not in BACKUP_GIANT	
Not in BACKUP_GIANT_LOP	
Exclude Galactic plane	(($b > -0.139\,l + 25°$ AND $l \leqslant 180°$)
	OR ($b > 0.139\,l - 25°$ AND $l > 180°$)
	OR ($b < -0.139\,l + 25°$ AND $l > 180°$)
	OR ($b < 0.139\,l - 25°$ AND $l \leqslant 180°$))

excludes the Galactic plane according to the prescription described in Table 1.

The final MWBP target samples consist of 45.6M, 1.85M, 26.1M, 25.0M, and 33.4M stars in the `BACKUP_BRIGHT`, `BACKUP_GIANT`, `BACKUP_GIANT_LOP`, `BACKUP_FAINT`, `and BACKUP_VERY_FAINT` target classes, respectively. These target classes and the overall selection for the MWBP are summarized in Table 1. These five candidate classes are targeted in the following prioritized order: `BACKUP_GIANT>BACKUP_BRIGHT>BACKUP_GIANT_LOP>BACKUP_FAINT>BACKUP_VERY_FAINT`.

3. Tiling Strategy

DESI is capable of simultaneously obtaining spectra of targets distributed over a 3.2 deg diameter circular field of view (T. N. Miller et al. 2024; C. Poppett et al. 2024). DESI defines a "tile" as a single pointing of the instrument at a particular location on the sky, with a fixed set of targets.

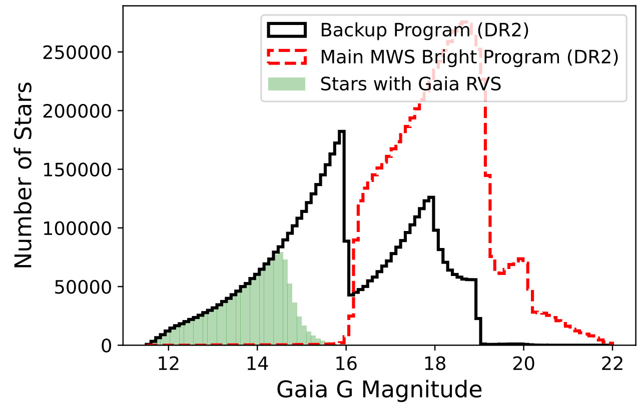

Figure 2. The Gaia *G*-band magnitude distributions of the spectroscopically observed targets in the MWBP (black histogram) and the MWS (red dashed histogram). The subset of stars with radial velocity measurements from Gaia Radial Velocity Spectrometer are shown by the shaded green histogram. The DESI histograms are constructed from the targets observed during (approximately) the first three years of survey operations and which will be included in the second DESI Data Release (DR2).

Details of the tiling strategy for the DESI main survey have been presented by E. F. Schlafly et al. (2023). The footprint for the MWBP is an expanded version of the DESI footprint, extending south to decl. $\delta \geqslant -30°$ and covering the range of Galactic latitudes described in Table 1 (see also Figure 3). The MWBP uses a tiling of 2657 tiles to cover this entire expanded footprint of more than 21,000 deg^2. This tiling is equivalent to the first layer ("Pass 0") of the DESI Main Survey but extends over the larger footprint of the MWBP. By design, the MWBP tiles do not overlap each other (see Figure 3). This first pass (i.e., "Pass 0") tiling of the Backup Program, when completed, will result in spectra of ≈10 million Gaia sources (compared with the ≈9 million stars observed by the end of the MWS). Depending on the completion rate of this first tiling, and the extension of the DESI Survey beyond its current 5 year program, we will add more passes to fill in the gaps in the single layer tiling and increase the spectroscopic completeness of the targets.

The fiber assignment for a given tile is done on the fly just prior to its observation (see Section 5.6 of E. F. Schlafly et al. 2023). Briefly, for each tile, sources are selected from the MWBP target catalogs and prioritized as described in the previous section. The process of assigning a fiber to a target is complex. Targets are assigned to fibers starting with the highest priority target and proceeding downwards in priority, until all targets have been assigned or no positioners can reach any remaining targets without colliding with a previously assigned target. Since MWBP targets range over a wider footprint than the DESI Main dark- and bright-time surveys, extending beyond the region covered by the Legacy Surveys imaging (see A. Dey et al. 2019), standard stars for MWBP tiles are selected from the Gaia catalog as described in Section 4.2 of A. D. Myers et al. (2023; i.e., the `GAIA_STD_BRIGHT, GAIA_STD_FAINT` target classes). If there are any target-of-opportunity (TOO) triggers, these are also added during fiber assignment, with higher priority than the MWBP targets. TOO triggers are rare on tiles observed during backup conditions; for example, the entire DESI Data Release 1 (DR1) release only contains six (98) such targets.

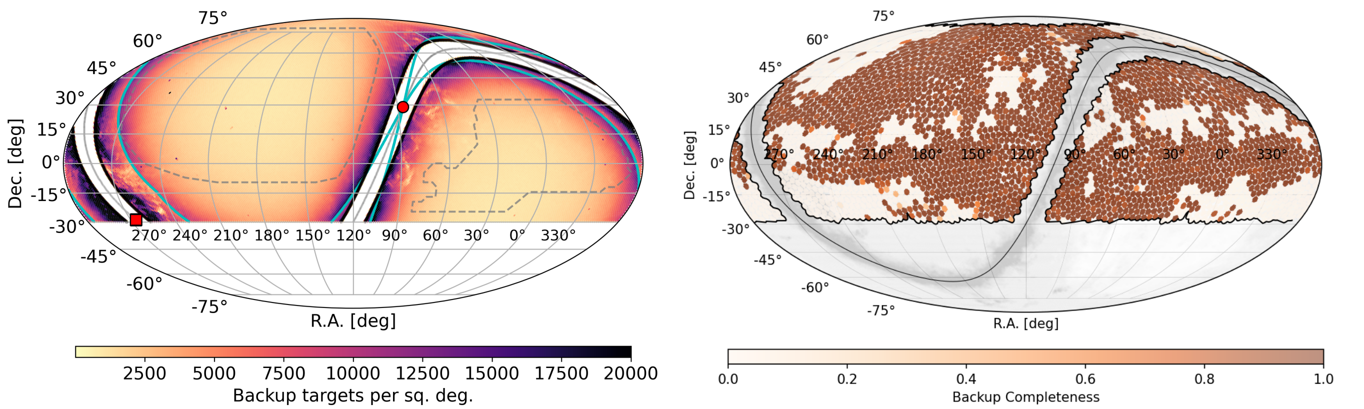

Figure 3. Left: The footprint of the MWBP. The cut at Galactic latitude $|b| \approx 7^\circ$ represents the boundary of the MWBP footprint for the `BACKUP_BRIGHT`, `BACKUP_GIANT`, and `BACKUP_GIANT_LOP` target classes, and the cyan solid lines show the variable b limits of the `BACKUP_FAINT` and `BACKUP_VERY_FAINT` selections (see Table 1). The footprint of the MWBP reaches to much lower Galactic latitudes (roughly $|b| \gtrsim 7^\circ$) than the MWS, which is shown by the gray dashed lines. The sky density of all potential MWBP targets is shown by the color scale. The Galactic center and anticenter are marked by a red square and circle, respectively. Right: Areal completeness of the MWBP as of 2025 March 1. The colorbar shows the completeness as a fraction of the nominal exposure time of $t_{\rm eff} = 60$ s; the red (and darker) dots represent tiles where the depth is at least 85% of the nominal depth. Nearly 70% of the tiles defined for the MWBP have been observed to this depth. The jagged black contour represents the true boundary of the edge tiles, and therefore the expected coverage of the footprint once the MWBP is complete.

The fiber assignment process typically results in approximately 4000 MWBP targets per tile, a number which varies with Galactic latitude, with the highest latitude tiles having as few as ≈3000 science targets per tile. Unlike tiles for the DESI Main bright survey (where targeting is prioritized for galaxy targets from the Bright Galaxy Survey), MWBP tiles contain almost exclusively stellar targets.

Although candidate targets are selected across the entire footprint using the criteria defined in Table 1, the tile selection is further restricted to tiles with centers satisfying the Galactic latitude limit $|b| \gtrsim 7^\circ$ and the decl. range $-28.5^\circ < \delta < 80^\circ$. This results in targets in the top three priority categories (i.e., `BACKUP_GIANT`, `BACKUP_BRIGHT`, and `BACKUP_GIANT_LOP`) being included over the full footprint down to $|b| \gtrsim 7^\circ$, but the two filler samples (i.e., `BACKUP_FAINT` and `BACKUP_VERY_FAINT`) being further restricted by the longitude-dependent Galactic latitude cut described in Table 1.

4. Observations and Strategy

The observational strategy for all parts of the DESI survey is described in detail in E. F. Schlafly et al. (2023). Here, we briefly describe the parts relevant to the triggering of the MWBP and the actual range of conditions that result from the strategy.

4.1. Observing Speed and Triggering Strategy

During a night when the instrument is on sky and observing, the observing software continuously computes the "survey speed," a dimensionless quantity that is related to the efficiency of observing a given tile under the current conditions. DESI defines the survey speed S as the rate of accumulation (per elapsed second) of effective exposure time, where the effective exposure time ($t_{\rm eff}$) is the time required to reach the required signal-to-noise ratio (SNR) in "nominal" photometric, zenith-observing conditions of $1\farcs1$ seeing, r-band sky brightness of 21.07 AB mag per square arcsec, and no extinction by Galactic dust. S can vary between zero (when the observation of a given tile is completely prevented due to clouds) to ≈2.5 under excellent conditions (see E. F. Schlafly et al. 2023, for details). The MWBP is executed during twilight (typically between ∼12° and 18° twilight, i.e., before it is dark enough for DESI Main Survey observations) and during times of poor weather (i.e., when the transparency, seeing, sky brightness, or some combination of these conditions are poor). The MWBP observations are triggered by software, with only occasional overrides by the lead observing scientist (i.e., the individual at the telescope who is responsible for the observations on any given night) when $S \leqslant 0.08$.

While S is not recorded for each spectrum, the average speed during the observation of a given source can be reconstructed from the DESI catalog data as follows:

$$\bar{S} = t_{\rm eff} \times f_{EBV} \times X^{1.75}/t_{\rm exp} \quad (4)$$

where $t_{\rm eff}$ is the effective exposure time defined above; $f_{EBV} = 10^{1.732E(B-V)}$ is the scaling factor applied for the Galactic extinction at the location of the tile, X is the airmass at the time of observation, and $t_{\rm exp}$ is the actual exposure time (see E. F. Schlafly et al. 2023, for details).[67] Figure 4 shows the resulting distribution of the average observing speed $\bar{S}$ for the MWBP and a comparison to the observing speed distributions for the DESI Main bright-time Milky Way Survey and the DESI Main dark-time Cosmology Survey (see also Figure 6 of E. F. Schlafly et al. 2023).

Since low observing speeds can result from a wide range of conditions, the MWBP observations can be triggered for a variety of reasons. Figure 5 shows the distribution of the observing conditions during which MWBP observations have been made. Although the MWBP observations span a wide range, most MWBP observations are triggered in conditions of either poor seeing (FWHM $\gtrsim 2''$), poor transparency ($\lesssim$0.3),

[67] Since the MWBP reaches low Galactic latitudes with regions of high extinction, the inclusion of the f_{EBV} term results in long plan exposure times for these fields. Hence, for all tiles observed after 2024 October 22, the term f_{EBV} was dropped from the observing speed estimate used at the telescope when exposing on MWBP tiles. This will slightly decrease the resulting $t_{\rm eff}$ for observations after this date, especially in regions of high Galactic extinction, but does not affect any observations included in the DESI DR1 and DR2 releases.

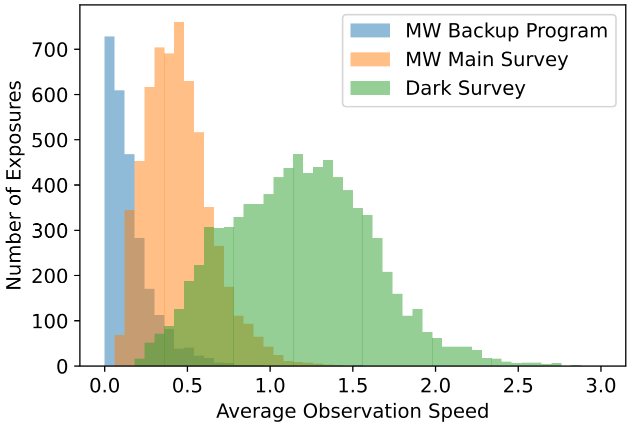

Figure 4. Distribution of average observing speed $\bar{S}$ (see text) for the MWBP (Blue histogram), MWS (orange histogram), and the DESI Main dark-time Cosmology Survey (green histogram) exposures.

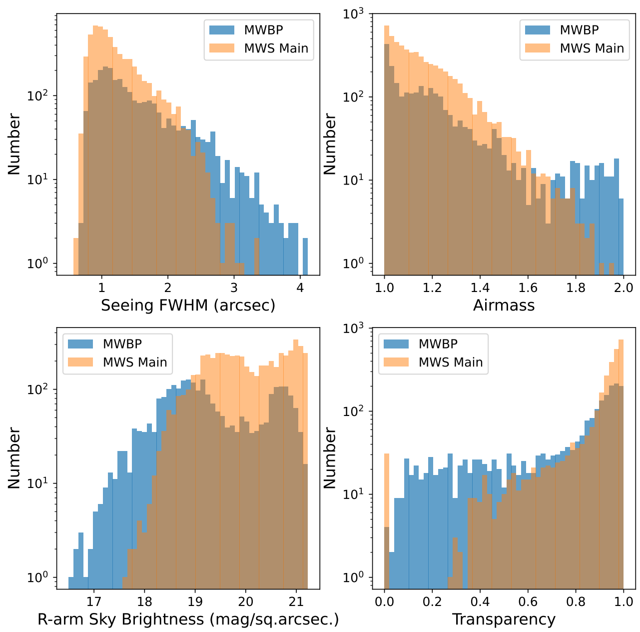

Figure 5. Distribution of sky conditions for the exposures taken for the MWBP (blue) and the MWS (orange). The four panels (clockwise from top left) show the seeing FWHM, airmass, transparency, and r-band sky brightness.

bright sky ($\gtrsim$19 mag arcsec^{-2}), or high airmass ($\gtrsim$1.5), or a combination of these.

When the conditions appropriate for the MWBP occur, tiles are scheduled to be observed automatically by the Next Field Selector (NFS) based on a number of parameters, including the observing speed, time of night, slew time, tile priority, moon location, etc. (see Section 5.5 of E. F. Schlafly et al. 2023, for details). Repeat visits to a specific tile to complete the observations do not occur on the same night.

4.2. Resulting Exposure Times

Tiles for the MWBP are observed with an effective exposure time goal of $t_{\rm eff} = 60$ s. This depth was chosen to ensure that all stars with $G < 16$ mag and (BP $-$ RP) $>$ 0.5 mag would have radial velocity measurements to better than $\approx$1 km s^{-1}. Since the conditions can be quite poor (and perhaps rapidly varying) for the MWBP, the range in effective time for any given exposure can vary significantly. Some exposures only result in advancing this time by 1 s (!) of effective time, whereas a few exposures may actually result in deeper observations than needed. Since individual exposure times are limited to 10 minutes, typically many exposures are needed to achieve the goal time.

The resulting distribution of exposure times is shown in Figure 6. Compared to the goal of $t_{\rm eff} = 60$ s, $\sim$80% of the exposures have $t_{\rm eff} < 60$ s, with a small number of exposures being overexposed (due to the conditions changing rapidly during the exposure). However, actual exposure times per observation of more than $\sim$10 minutes are typically needed to achieve this effective exposure time distribution, with the median value of the ratio of $t_{\rm eff}/t_{\rm exp} \approx 0.051$.

This strategy results in many repeat observations for individual sources until at least 85% of this exposure time ($\approx$51 s) is achieved. The distribution of the number of observations per tile achieved in the MWBP is shown in Figure 7.

5. Data from the MWBP

5.1. Current Status

The MWBP observations obtained thus far represent only $\approx$9% of all of the observing time used by DESI. The DESI Main Survey began on 2021 May 14 and the first MWBP exposure was obtained on 2021 April 4. As of 2025 March 1, DESI has observed nearly 1937 ($\approx$73%) of the planned 2657 MWBP tiles.

5.2. Data Availability

The DESI project schedules periodic public releases of the spectroscopic data and associated value-added catalogs. The data from the MWBP have been included as part of the DESI Early Data Release (EDR) and DR1. EDR contains 148k MWBP spectra taken during DESI Survey Validation phase and the One Percent Survey (DESI Collaboration et al. 2024). DR1 includes 1.2M MWBP spectra obtained during the first 13 months (i.e., 2021 May 14 through 2022 June 13) of DESI operation (DESI Collaboration et al. 2026). DR2, which will encompass the first 3 years (i.e., 2021 May 14 through 2024 April 9) of DESI survey spectroscopy and will contain 4.9M spectra of MWBP targets, is scheduled for release by early 2027. The DR1 release represents spectra collected from 327 unique tiles (i.e., $\approx$12% of the total footprint, or $\approx$3000 deg^2); the DR2 release will increase this to 1310 tiles (i.e., $\approx$49% of the footprint). We refer the reader to DESI Collaboration et al. (2024, 2026) for the details of the specific data releases. The sky coverage of the MWBP in the DR1 and DR2 releases is shown in Figure 8. The number of spectra observed in each Target Class within each DESI Data Release is shown in Table 2.

The MWBP targets can be identified within any of these data releases by selecting sources according to the tags `SURVEY="main"` and `PROGRAM="backup."` For comparison, the MWS targets can be found selecting `SURVEY="main"` and `PROGRAM="bright."` Targets for each of the five target class described in Table 1 can be identified using the targeting bit values [58, 59, 60, 61, 62] recorded in the `MWS_TARGET` tag for the [`BACKUP_GIANT_LOP`, `BACKUP_GIANT`, `BACKUP_BRIGHT`, `BACKUP_FAINT`, `BACKUP_VERY_FAINT`] target classes, respectively (see also Appendix B4 of DESI Collaboration et al. 2026). The DESI MWBP spectra constitute $\approx$22% (33%) of the MWS sources in the DESI DR1 (DR2) release.

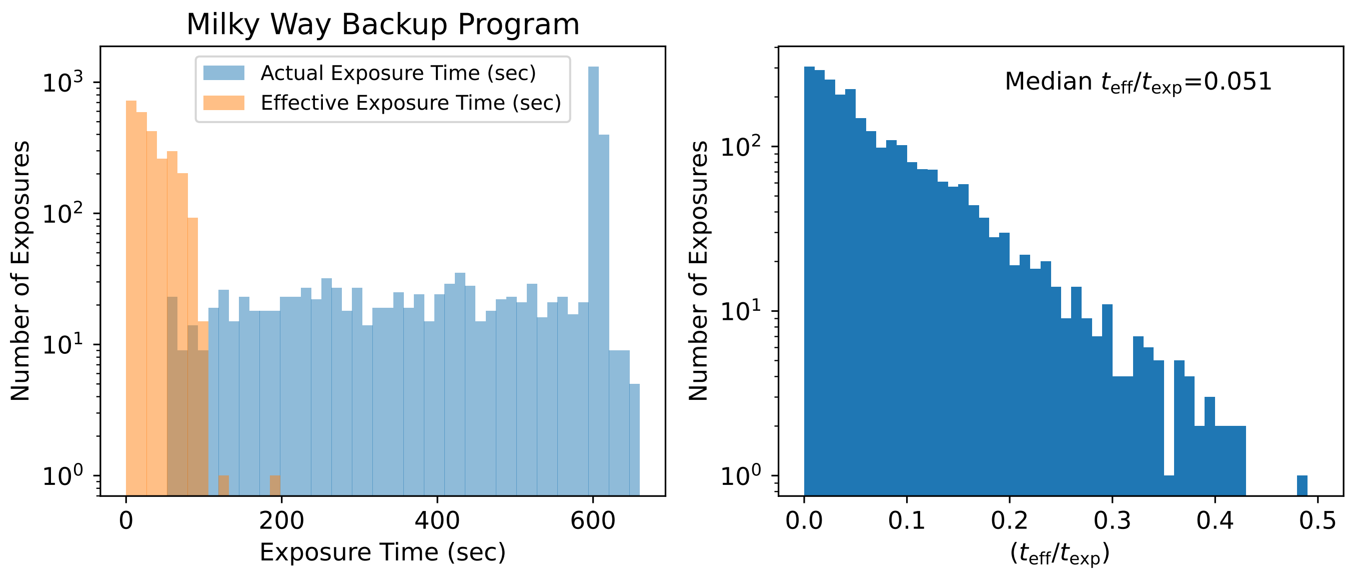

Figure 6. Left: Distribution of the actual exposure time (blue) and the effective exposure time (orange) for the MWBP exposures. Right: The distribution of the ratio of the effective exposure time (t_{eff}) to the actual exposure time (t_{exp}) for each observation.

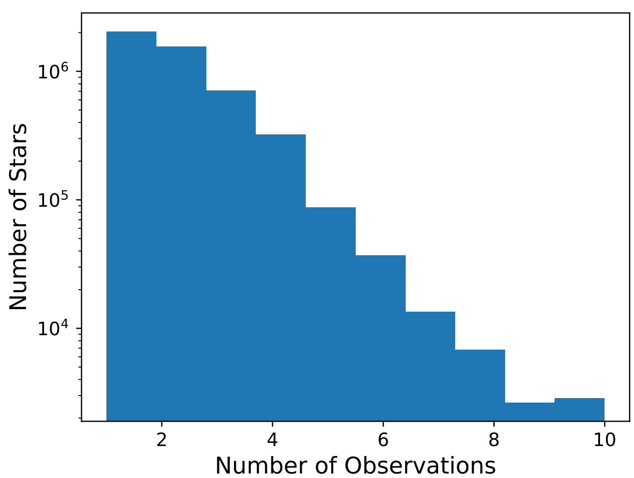

Figure 7. Distribution of the number of observations per target. Nearly 60% of the MWBP stars have more than one observation.

In what follows, we provide a broad description of the quality of the MWBP data, separating out, where useful, the spectra released in March 2024 as part of DR1 and the spectra that will be included in the DR2 release. The pipeline processing associated with DR1 is described in full detail by DESI Collaboration et al. (2026); the processing associated with DR2 will be described in a future paper. For additional details regarding the spectra of stars in DR1, please see the detailed description of the DESI Stellar Catalog (released as the DR1 MWS Value-Added Catalog) in S. Koposov et al. (2026).[68]

5.3. Calibrations and Reductions

The data are reduced using the standard DESI spectroscopic pipeline described in J. Guy et al. (2023). Given the wide range of (typically poor) observing conditions during which MWBP spectra are obtained, individual exposures can vary significantly in their SNR. When the median SNR < 2 for the standard stars in a given exposure, the pipeline does not attempt to derive a full reconstruction of the throughput per wavelength element from the standard stars in the observation, but instead reverts to using a predefined calibration vector normalized to the broad-band flux of the stars. While this mode is implemented as a standard part of the pipeline for the entire survey, it tends to be applied more often in the case of MWBP spectra (see also DESI Collaboration et al. 2024, for further details).

The reduced and calibrated spectra are analyzed using Redrock (A. Anand et al. 2024; S. Bailey et al. 2026, in preparation), a template-based principal component analysis (PCA) method, to measure redshifts and determine spectral classifications (in three broad categories of `STAR`, `QSO`, or `GALAXY`) for all sources. Although the vast majority of MWBP sources are stars, the selection described in Table 1 does result in a small number of extragalactic sources (see Section 5.6 for more details).

After the Redrock processing is complete, we run two additional pipelines (Radial Velocity Spectrometer, RVS, and SP, based on RVSpecFit by S. Koposov 2019 and FERRE by C. Allende-Prieto & Apogee Team 2023, respectively), which fit stellar atmosphere models to the spectra and compute more accurate radial velocities, stellar parameters (effective temperatures (T_{eff}), surface gravities ($\log g$), metallicities, $[\alpha/\mathrm{Fe}]$, etc.), and a few elemental abundances for all the sources in the MWBP (see S. E. Koposov et al. 2024; S. Koposov et al. 2026, for details). The sources are also crossmatched to the Gaia DR3 catalog. These quantities are included as part of the DESI Stellar Catalog, a Value-Added Catalog released as part of the DESI EDR (DESI Collaboration et al. 2024; S. E. Koposov et al. 2024) and DR1 (DESI Collaboration et al. 2026; S. Koposov et al. 2026).

5.4. Data Quality and Velocity Uncertainties

Figure 9 shows the distribution of formal radial velocity uncertainties as a function of the Gaia G and (BP − RP) colors as measured in the DESI DR2 dataset. The bulk of the sample

[68] The DESI DR1 Stellar Catalog is available at https://data.desi.lbl.gov/doc/releases/dr1/vac/mws/.

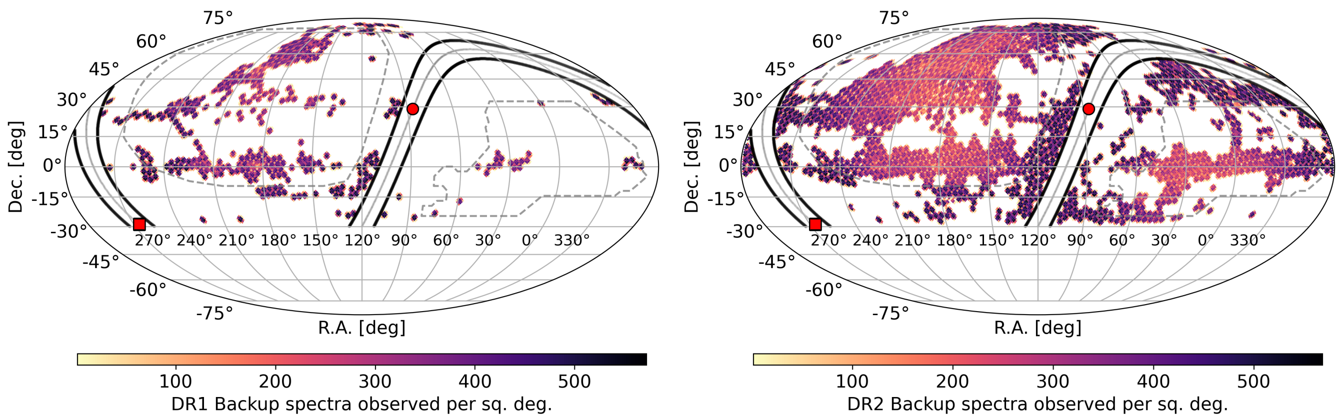

Figure 8. The sky density and distribution of MWBP spectra in the DESI DR1 dataset (left) and the future DR2 dataset (right). The gray dashed line shows the slightly smaller footprint covered by MWS. The Galactic center and anticenter are marked by a red square and circle, respectively, and the solid black lines represent the MWBP Galactic latitude limit of $|b| = 7°$.

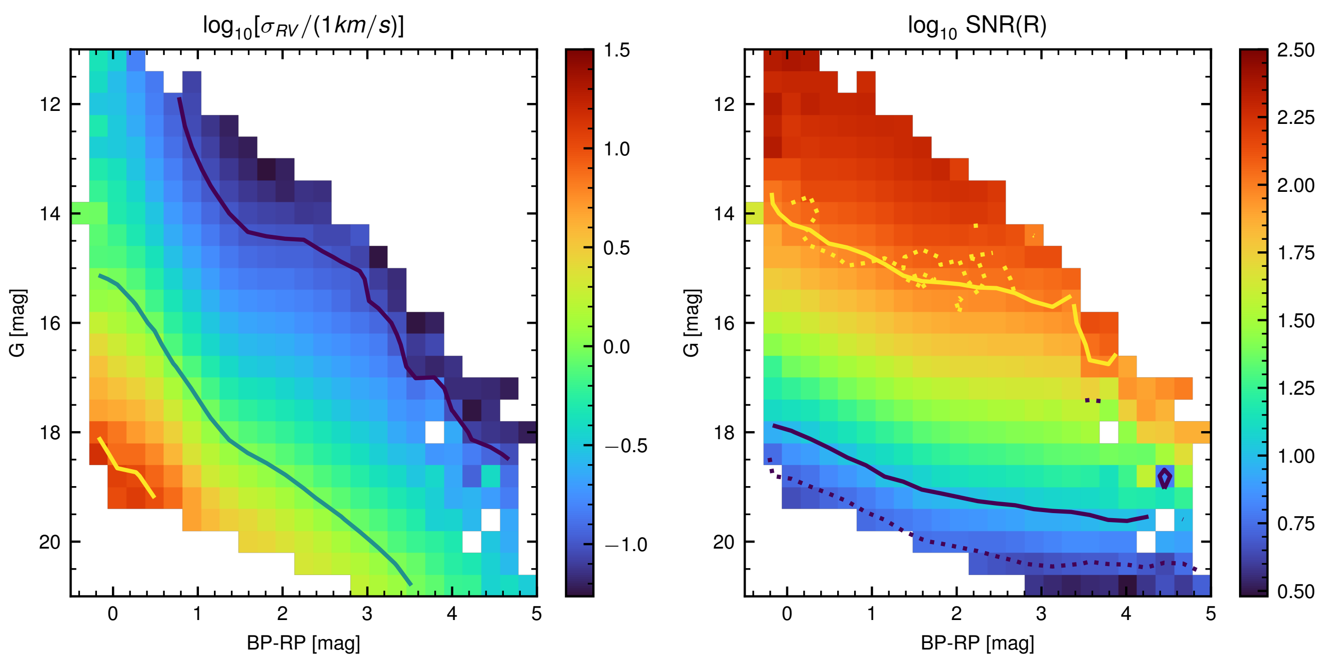

Figure 9. Left panel: Formal radial velocity uncertainties as a function of Gaia G magnitude and (BP − RP) color. The colorbar shows $\log_{10}(\sigma_{RV}/[1\ \mathrm{km\ s^{-1}}])$, and lines show contours of constant radial velocity uncertainty of 0.1,1 and 10 km s^{-1} (dark blue, light blue, and yellow respectively). Right panel: Median SNR per pixel in the R-arm of the spectrograph as a function of Gaia color and magnitude. The solid lines show contours corresponding to SNR = 10 (blue) and SNR = 100 (yellow). The dotted lines show the same SNR contours but for the bright-time MWS.

Table 2
Target Class Distribution Across Different Data Releases

Target Class	All Targets[a]	Tile Targets[b]	DR1	DR2	Total[c]
BACKUP_BRIGHT	45,677,684	22,472,468	636,850	2,832,416	6,260,000
BACKUP_GIANT	1,853,482	1,382,372	117,882	464,857	1,000,000
BACKUP_GIANT_LOP	26,127,761	17,245,747	148,239	573,094	1,220,000
BACKUP_FAINT	24,958,299	18,406,150	196,848	664,914	1,210,000
BACKUP_VERY_FAINT	33,392,580	24,001,223	116,580	369,782	640,000
Total MWBP Targets	132,009,808	83,507,960	1,216,399	4,905,063	10,330,000
MWS		30,470,033			9,890,000

Notes.
[a] All targets at decl. $> -30°$.
[b] Targets covered by the MWBP tiles.
[c] Approximate number of stars anticipated at the completion of the survey, based on mock fiber assignment for the full MWBP tiling.

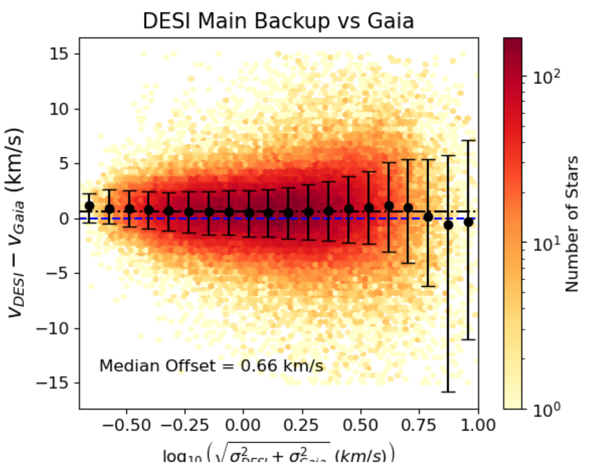

Figure 10. Comparison between MWBP and Gaia radial velocity measurements for ≈10^5 stars from the DESI DR2 release with >20σ Gaia RVS measurements. The blue dashed line shows $\delta(v) \equiv v_{\rm DESI} - v_{\rm Gaia} = 0$, and the black points show the median value of the offset in bins of total error. The vertical bars show the range between the 16th and 84th percentiles. The dashed black line shows the median value of 0.66 km s^{-1}, which represents the overall systematic offset between the DESI DR2 and Gaia radial velocity values.

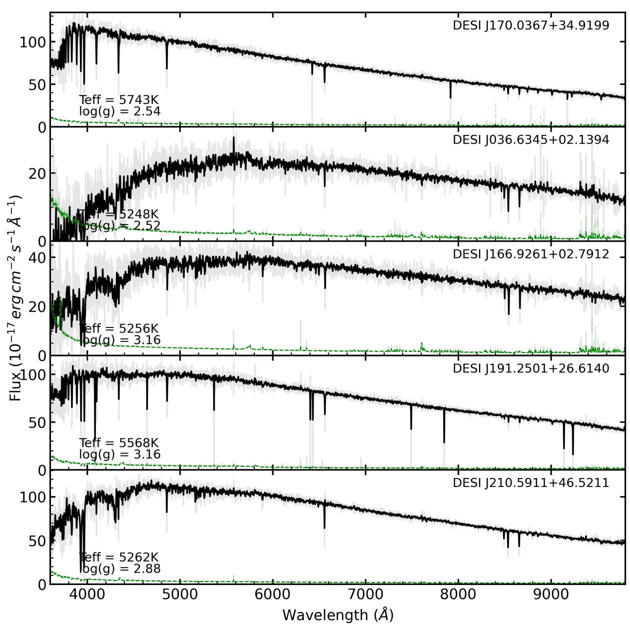

Figure 11. Spectra of five random giant stars of target class `BACKUP_GIANT` from the MWBP. In each panel, the light gray and green lines show the unsmoothed flux and noise spectra, while the black and darker green lines show the corresponding spectra smoothed by a 0.8 Å Gaussian kernel.

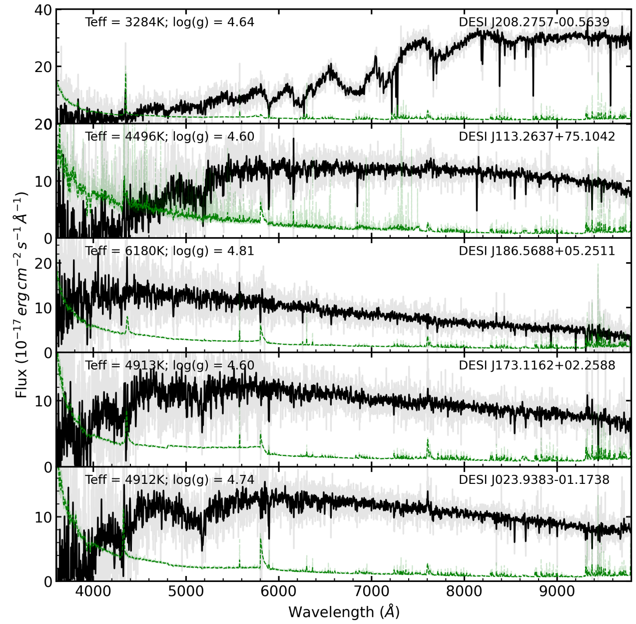

Figure 12. Spectra of five random stars of target class `BACKUP_VERY_FAINT` from the MWBP. In each panel, the light gray and green lines show the unsmoothed flux and noise spectra, while the black and darker green lines show the corresponding spectra smoothed by a 0.8 Å Gaussian kernel.

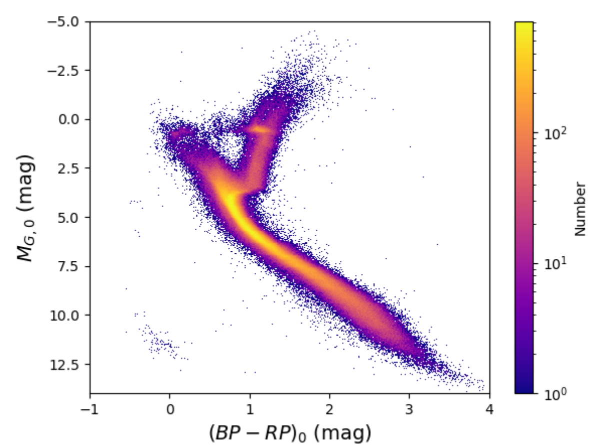

Figure 13. Extinction-corrected observational Hertzsprung–Russell diagram of stars from the MWBP, constructed using distance estimates from the SpecDis Value-Added Catalog (S. Li et al. 2025).

has velocity measurement uncertainties of ⩽5 km s^{-1}, with only the bluest (i.e., (BP − RP) ≲ 1 mag) and faintest (i.e., G ≳ 18 mag) populations having larger uncertainties (i.e., ≳10 km s^{-1}). In addition to the formal uncertainties, a comparison of repeat observations of sources show a systematic floor to the noise level of ≈2 km s^{-1} for MWBP spectra, higher than the noise floor of ≈1 km s^{-1} observed for the MWS (for a detailed discussion, please see DESI Collaboration et al. 2025c; S. Koposov et al. 2026).

In the process of analyzing the velocity accuracy of the data from the MWBP included in the DESI DR1 release, a problem was identified with the wavelength calibration of some exposures. Due to the increased continuum sky brightness and the algorithm used to correct the wavelength solution by using sky lines, incorrect offsets were applied, which resulted in some exposures having large (in rare cases up to ∼20 km s^{-1}) velocity zero-point offsets. This algorithm has since been modified to be less affected by high sky brightness and has been corrected for DESI DR2. However, the DESI DR1 radial velocities for all sources have a median offset of $\Delta V \equiv V_{\rm DR2} - V_{\rm DR1} \approx 1$ km s^{-1}, with a scatter of $\sigma(\Delta V)$ ≈ 2.6 km s^{-1}. In addition, the distribution of ΔV is asymmetric and has significant non-Gaussian tails, with ≈8% of sources having $|\Delta V| \geqslant 10$ km s^{-1} (see S. Koposov et al. 2026, for details). When using the MWBP data from DR1, we caution the reader to use the correction from S. Koposov et al. (2026) and assume additional systematic errors <5–10 km s^{-1}, depending on the field location (see S. Koposov et al. 2026, for details).

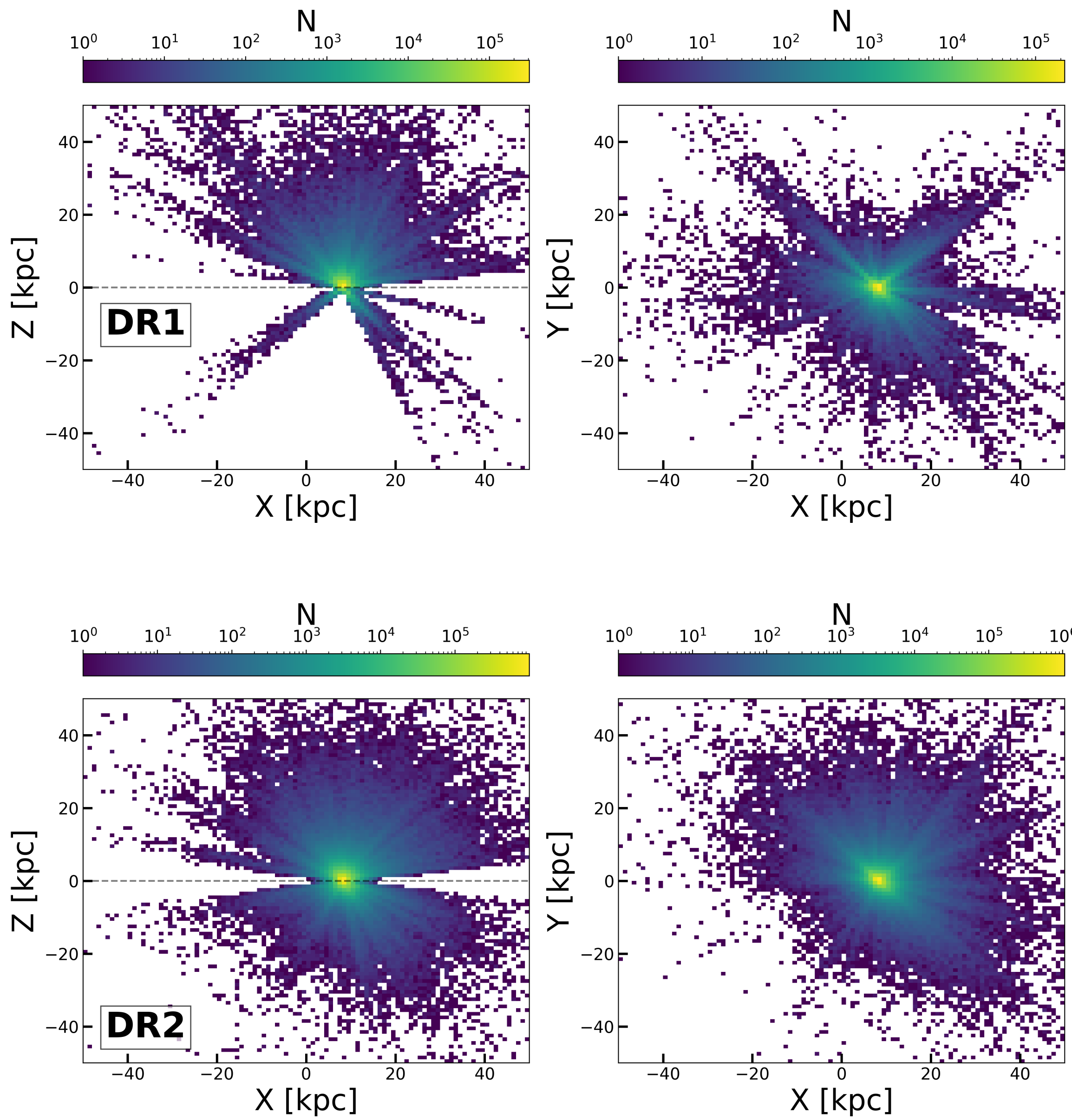

Figure 14. The projection of spectroscopically observed MWBP targets in Galactocentric coordinates (X, Y, Z) of the MWBP based on distances from the SpecDis Catalog (S. Li et al. 2025), color coded by number density of spectra. The top and bottom panels show the density distribution of stars for the DESI DR1 and DR2 data releases, respectively, which represent ≈12% (DR1) and nearly 50% (DR2) of the total MWBP footprint (see left panel of Figure 8).

5.5. Gaia RVS Survey Comparison

The MWBP radial velocities agree well with the velocities reported by the Gaia RVS. Gaia RVS undertook high-resolution ($R \equiv \lambda/\delta\lambda \approx$ 11,500) spectroscopy in a narrow wavelength range (8460–8700 Å) of roughly 5.6 million bright ($G \lesssim 14$ mag) stars (A. Recio-Blanco et al. 2023). Approximately 25% of all the sources observed by MWBP overlap with these; in contrast, <7% of sources in the MWS have Gaia RVS measurements. For the sample that overlaps, DESI contributes spectral information spanning the entire 3600–9800 Å wavelength range. Figure 10 compares the MWBP and Gaia radial velocities for stars from the DESI DR2 release with $\geqslant 20\sigma$ Gaia radial velocity measurements. These show a small residual systematic offset of $\delta(v) \equiv v_{\rm DESI} - v_{\rm Gaia} \approx 0.7\,{\rm km\,s^{-1}}$, with median 16th and 84 percentiles of $\approx -2.4\,{\rm km\,s^{-1}}$ and $\approx +2.3\,{\rm km\,s^{-1}}$, respectively.

5.6. Scientific Yield

As of 2025 March 1, DESI has completed roughly 70% of the tiles for the MWBP, resulting in spectra of >7 million stellar targets. DESI DR1 presents catalogs and spectra of 1.2M of these. The DESI DR1 Stellar Catalog presents radial velocities, effective temperatures $T_{\rm eff}$ surface gravities (log g), metallicities, and a few elemental abundances of the stars derived using the RVS and SP pipelines (S. E. Koposov et al. 2024; S. Koposov et al. 2026).

From the RVS results, we find the yield of giant stars (sources with $\log g < 4$) is ≈21% for the BACKUP_GIANT targets and ≈ 14% for the BACKUP_GIANT_LOP targets. Example spectra of these giant stars are shown in Figure 11. In addition, about 15% of the BACKUP_BRIGHT stars are classified as giants. Figure 12 shows five example spectra of

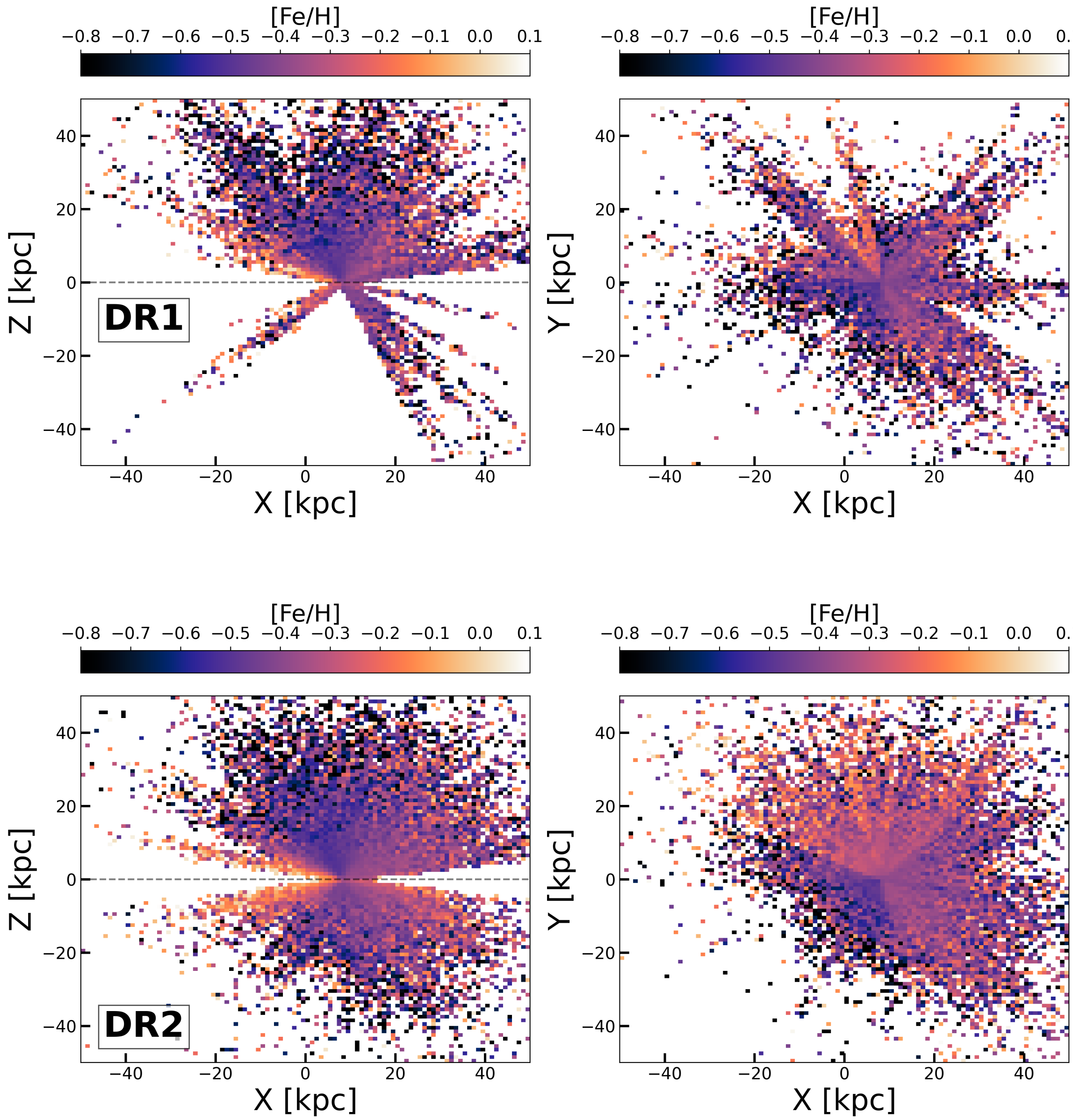

Figure 15. The distribution of metallicities of spectroscopically observed MWBP targets shown in Galactocentric coordinates (*X*, *Y*, *Z*) of the MWBP for the DESI DR1 and DR2 data releases, respectively. Distance estimates are based on the SpecDis Catalog (S. Li et al. 2025) and metallicities are from the RVS estimates (S. E. Koposov et al. 2024; S. Koposov et al. 2026).

the BACKUP_VERY_FAINT target class to illustrate the data quality and kinds of sources.

The Milky Way Survey SpecDis Value Added Catalog (SpecDIS VAC; S. Li et al. 2025) presents distance estimates for nearly all stars in the DESI DR1 release (including MWBP targets) based on a neural network approach. A future paper will present the SpecDIS VAC for DESI DR2. Figure 13 shows the observational Hertzprung–Russell diagram in the Gaia absolute *G*-band magnitude versus (BP − RP) color plane for the ≈0.76 million MWBP stars from DESI DR1 with distance estimate uncertainties $\lesssim$25%. The Gaia magnitudes and colors have been corrected for Galactic dust extinction using the coefficients derived by Gaia Collaboration et al. (2018a) and the $E(B-V)$ estimates derived by D. J. Schlegel et al. (1998) with corrections from E. F. Schlafly & D. P. Finkbeiner (2011). Figure 13 demonstrates that the MWBP covers most of the stellar locus, including a small number of white dwarfs.

Figures 14 and 15 present the spatial distribution of the MWBP DR1 and DR2 samples in Galactocentric coordinates, color coded by number density and metallicity. The conversion to a Galactocentric frame assumed a Solar velocity of [11.1, 248.5, 7.25] km s^{-1} (R. Schönrich et al. 2010; M. J. Reid & A. Brunthaler 2020), a Galactocentric distance of 8.178 kpc (GRAVITY Collaboration et al. 2019), and an *Z*-distance offset of 20.8 pc (M. Bennett & J. Bovy 2019). The distance and metallicity estimates are from the SpecDis VAC and DESI DR1 Stellar Catalog, respectively (see, e.g., S. Li et al. 2025; S. Koposov et al. 2026). The MWBP stars are primarily located well within 15 kpc of the Sun (top panels). For DR1, the 50th, 84th and 95th percentiles of the distance distribution are 1.67 kpc, 4.9 kpc, and 6.6 kpc, respectively,

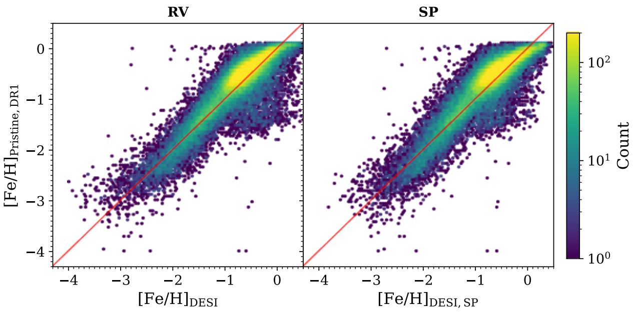

Figure 16. Comparison of the photometrically derived metallicities in the PRISTINE DR1 catalog (N. F. Martin et al. 2024) with the spectroscopic metallicity estimates from the MWBP observations of the same stars based on the RVS (left) and SP (right) pipelines as reported in the DESI DR1 Stellar Catalog (S. E. Koposov et al. 2024; DESI Collaboration et al. 2026; S. Koposov et al. 2026). The solid red line in both panels is a 1–1 line, not a fit.

with nearly 31.5K stars at distances >10 kpc. The stars also span a range in metallicity (bottom panels). For DR1, the 16th, 50th, and 84th percentiles of the metallicity distribution are [Fe/H] ≈ -0.77, -0.39, and -0.06. While DESI DR1 mainly samples stars at $Z > 0$, DR2 will extend the coverage to the southern Galactic cap.

5.6.1. Comparison with the PRISTINE Survey

The MWBP metallicities can also be used to validate photometric metallicities derived from narrow-band imaging surveys. For example, the MWBP provides spectroscopic measurements for a significant population of stars measured by the PRISTINE Survey (E. Starkenburg et al. 2017; N. F. Martin et al. 2024), which uses MegaCam on the Canada–France–Hawaii Telescope to map the northern sky in a narrow-band CaHK filter during poor weather time, an effort not unlike MWBP. Data Release 1 of the PRISTINE Survey reports photometric and astrometric measurements for approximately 6.38M stars over 6500 deg^2, along with photometrically estimated metallicity measurements (see N. F. Martin et al. 2024). The DESI DR1 and DR2 data overlap with this sample over $\approx$925 deg^2 and $\approx$3300 deg^2, respectively. Figure 16 compares the photometric metallicities in the PRISTINE DR1 catalog with the (more accurate) spectroscopic metallicities from the DESI DR1 Stellar Catalog (DESI Collaboration et al. 2026; S. Koposov et al. 2026) for the stars meeting the quality criteria listed in N. F. Martin et al. (2024) and the quality criteria related to the SP pipeline described in S. E. Koposov et al. (2024). We confirm that the PRISTINE photometric metallicity estimates are generally quite good, with a scatter of 0.22 (0.23) dex compared to the SP (RVS) pipeline spectroscopic metallicities. However, PRISTINE metallicities are systematically more metal poor by 0.06 (0.05) dex compared to the DESI SP (RVS) metallicities, respectively. This offset decreases to 0.02 (0.01) dex below [Fe/H] < -2.0.

While these differences are small, we caution the reader that they are also much smaller than the accuracy of the DESI spectroscopic metallicities. S. Koposov et al. (2026) cross matches the stars in the DESI DR1 Stellar Catalog with those measured by the APOGEE (S. R. Majewski et al. 2017; Abdurro'uf et al. 2022), GALAH (G. M. De Silva et al. 2015; S. Buder et al. 2025), Gaia (Gaia Collaboration et al. 2016, 2018b; A. Recio-Blanco et al. 2023), and SAGA (T. Suda et al. 2008, 2011) surveys and finds that the DESI metallicity estimates show systematic offsets relative to the other surveys, which are different for giant and dwarf stars. Empirically correcting for these systematic offsets results in scatter of the DESI metallicity estimates of $\approx$0.1 dex.

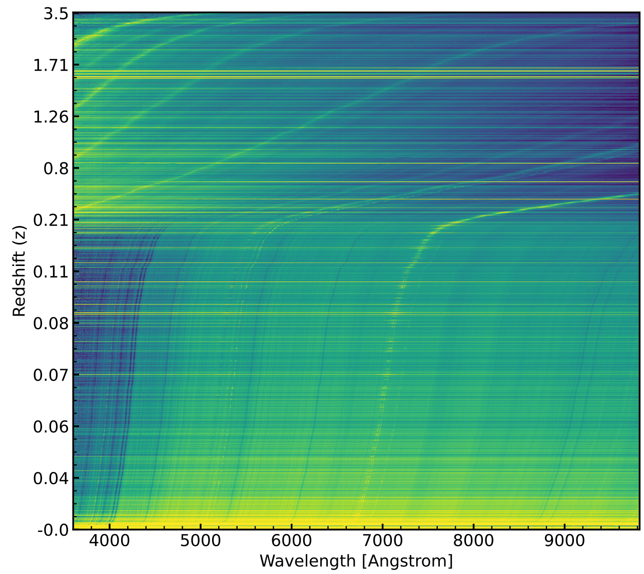

Figure 17. 5687 DESI spectra of primarily extragalactic sources from the MWBP, arranged in increasing redshift. For all of these spectra, the DESI Redrock pipeline produced $\geqslant 5\sigma$ redshift determinations, but the RVS pipeline failed to find a fit. Several emission and absorption features typical of galaxy and QSO spectra are seen tracking diagonally across the image with increasing redshift. A small number of the brightest horizontal lines are spectra of stars that are misclassified as spectral type `GALAXY` by Redrock.

5.6.2. Extragalactic Sources in MWBP

In addition to obtaining spectra of a large number of stars, the MWBP also obtains spectra of extragalactic sources that are included in the Gaia catalog. Of the 1.2M sources in the DESI DR1 release with reported reliable Redrock measurements (i.e., `ZWARN=0` and `DELTACHI2` $\geqslant$ 25), Redrock classifies 2743 ($\approx$0.23%) as spectral type `QSO` and 16,240 ($\approx$1.34%) as type `GALAXY`. The set classified by Redrock as spectral type `QSO` (which is based on broad-line quasar archetypes; e.g., DESI Collaboration et al. 2024) contains only a small number of misclassified sources (a few Carbon stars, unusual white dwarfs, and a handful of sources with calibration issues). Such QSO misclassifications are a minority: only 27 (<0.1%) of sources classified as `QSO` by Redrock are Galactic stars.

The set classified by Redrock as `GALAXY`, in contrast, includes a large fraction ($\approx$65%) of misclassified stars. These include reddened stellar sources, a handful of sources that show emission lines from interstellar or circumstellar gas, or stellar spectra that are poorly represented by the limited set of Redrock templates.

Galaxy and QSO spectra from the MWBP can generally be selected from the DR1 Stellar Catalog by identifying the sources that Redrock has confidently identified as a `GALAXY` or `QSO` spectral type (i.e., `ZWARN=0` and `DELTACHI2`$\geqslant$25), and for which the RVS fit results in warning flags (i.e., `RVS_WARN`$\neq$0). Figure 17 shows these spectra ordered by redshift, where the pattern of redshifting emission lines typical of galaxies (at $z < 1.6$) and quasars (at $z > 2$) is readily seen. This plot also shows some outliers (e.g., the two bright continuum spectra which can be seen near $z \approx 1.7$) which tend to be the stellar contaminants. Figure 18 shows the sources that

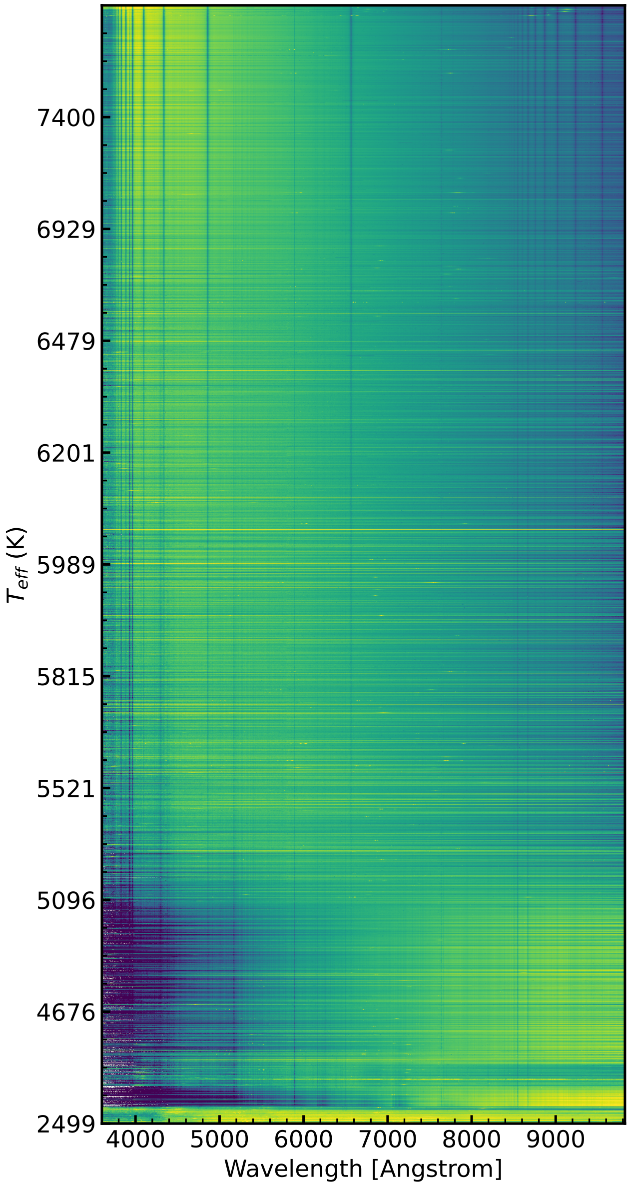

Figure 18. Spectra of 13,290 (primarily) stellar sources from the MWBP that were misclassified as spectral type GALAXY by the Redrock pipeline but for which the RVS pipeline found a good model fit. The sources are sorted by their effective temperature estimated by the RVS pipeline. Nearly all of the sources are stars, as evidenced by their (approximately) zero redshift absorption features. However, there are also several galaxies and QSOs visible within this set, which are identifiable by their emission signatures. The sources with the lowest estimated effective temperatures ($T_{\rm eff} < 3000$ K) are also likely sources with problematic RVS fits.

Redrock robustly identified as galaxies or QSOs, but for which the RVS model fits had no warning flags (i.e., RVS_WARN=0). Nearly all of these sources are indeed stars. However, close examination of Figure 18 reveals a small but significant number of galaxy and QSO emission lines scattered within the collection (e.g., several spectra which show emission lines at ∼7800 Å in the upper right quadrant of the plot).

Figure 19 shows examples of five rare objects observed by the MWBP, illustrating the range of astronomical gems produced by large spectroscopic surveys. The bottom two panels of Figure 19 show examples of QSO spectra from the MWBP; the top three panels show sources that were misclassified as type QSO by Redrock but which turn out to be rare stellar sources.

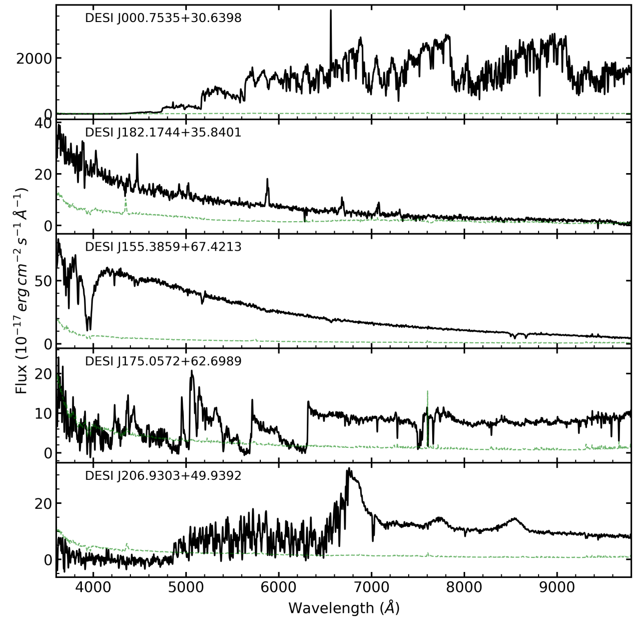

Figure 19. Smoothed spectra of a few rare gems from the MWBP. From top to bottom, the panels show a Carbon Star, a AM CVn type cataclysmic variable, a metal enriched white dwarf with strong Ca lines, a broad absorption line QSO at $z = 3.077$, and a high-redshift QSO at $z = 4.526$. The green lines show the noise level in these spectra.

6. Summary

We have presented an overview of the MWBP being carried out by DESI at the Mayall 4 m Telescope at the Kitt Peak National Observatory. The goal of the MWBP is to utilize twilight times (<18°) and poor weather conditions as efficiently as possible to supplement the MWS. Accordingly, the MWBP extends the observed range of targets to brighter magnitudes and lower Galactic latitude and decl. than that of the MWS. The final MWBP will cover more than 20,000 deg^2 at decl. $> -28\overset{\circ}{.}5$ and $|b| \gtrsim 7°$ and deliver spectroscopy of roughly 10 million stars.

The MWBP targets are selected from the Gaia catalog, prioritizing an unbiased sample of bright stars ($11.2 \leqslant G < 16$) and candidate halo giant stars ($16 < G \lesssim 19$) selected based on their Gaia (DR2) parallaxes. The MWBP has the advantage of obtaining multiple (low SNR) observations for many of the targets with nearly 60% of the MWBP stars having more than one epoch of observation. While the data are of poorer quality than the MWS for stars of similar magnitudes, the MWBP results in spectra with average R-arm SNR exceeding 100 for the brightest stars and delivers radial velocity measurements with a precision of $\approx$1 km s^{-1} for stars with Gaia $G \approx$ 18–19 mag (depending on color).

The DESI DR1 release, which represents (roughly) the first year of DESI survey observations, includes spectra of ≈1.2M unique MWBP targets, and covers ≈12% of the total footprint. The stellar measurements for the MWBP based on DR1 were released as part of the DESI DR1 Stellar Catalog and are described in S. Koposov et al. (2026). The survey has currently completed nearly 70% of its originally planned footprint and is likely to complete the original set of MWBP tiles within a year. Given the success of this program, we will likely continue it in future phases of the DESI project by increasing the density of the tiling and/or increasing the areal coverage as appopriate. The MWBP represents a good example of how to optimize the utility of poor weather time for ongoing and future spectroscopic surveys.

Acknowledgments

This material is based upon work supported by the U.S. Department of Energy (DOE), Office of Science, Office of High-Energy Physics, under Contract No. DE-AC02-05CH11231, and by the National Energy Research Scientific Computing Center, a DOE Office of Science User Facility under the same contract. Additional support for DESI was provided by the U.S. National Science Foundation (NSF), Division of Astronomical Sciences under Contract No. AST-0950945 to the NSF's National Optical-Infrared Astronomy Research Laboratory; the Science and Technology Facilities Council of the United Kingdom; the Gordon and Betty Moore Foundation; the Heising-Simons Foundation; the French Alternative Energies and Atomic Energy Commission (CEA); the National Council of Humanities, Science and Technology of Mexico (CONAHCYT); the Ministry of Science, Innovation and Universities of Spain (MICIU/AEI/10.13039/501100011033), and by the DESI Member Institutions: https://www.desi.lbl.gov/collaborating-institutions. Any opinions, findings, conclusions, or recommendations expressed in this material are those of the author(s) and do not necessarily reflect the views of the U. S. National Science Foundation, the U. S. Department of Energy, or any of the listed funding agencies. The authors are honored to be permitted to conduct scientific research on I'oligam Du'ag (Kitt Peak), a mountain with particular significance to the Tohono O'odham Nation.

This work has made use of data from the European Space Agency (ESA) mission Gaia (https://www.cosmos.esa.int/gaia), processed by the Gaia Data Processing and Analysis Consortium (DPAC, https://www.cosmos.esa.int/web/gaia/dpac/consortium). Funding for the DPAC has been provided by national institutions, in particular the institutions participating in the Gaia Multilateral Agreement.

This paper was begun at a workshop hosted by the Dunlap Institute for Astronomy and Astrophysics at the University of Toronto. We gratefully acknowledge the Dunlap Institute for their generous support and hospitality during the event, as well as Dunlap's Conferences and Workshop Funding that helped make this workshop possible. The Dunlap Institute is funded through an endowment established by the David Dunlap family and the University of Toronto.

A.P.C. is supported by Taiwan's National Science and Technology Council (113-2112-M-007-009) and a Yushan Fellowship awarded by the Taiwanese Ministry of Education (MOE-113-YSFMS-0002-001-P2). S.K. acknowledges support from the Science & Technology Facilities Council (STFC) grant ST/Y001001/1.

A.D.M. was supported by the U.S. Department of Energy, Office of Science, Office of High Energy Physics, under Award Number DE-SC0019022.

D.J.E. was supported by U.S. Department of Energy grant DE-SC0007881 and as a Simons Foundation Investigator.

Data Availability

The data required to generate the figures found in this article are available on Zenodo: doi: 10.5281/zenodo.19489156.

Facilities: Mayall (DESI), Gaia.

Software: Astropy (Astropy Collaboration et al. 2013, 2018, 2022), fitsio (https://github.com/esheldon/fitsio), healpy (A. Zonca et al. 2019), Matplotlib (J. D. Hunter 2007), NumPy (C. R. Harris et al. 2020), SciPy (P. Virtanen et al. 2020), SPARCL (S. Juneau et al. 2025).

Appendix

The nomenclature associated with the different DESI Stellar Surveys is presented in this Appendix and illustrated in Figure 20. The DESI Stellar Surveys consist of: (1) the MWS which is part of the DESI Main bright-time survey (and includes special samples of nearby stars, white dwarfs, RR Lyrae, and blue horizontal branch stars), discussed in detail in A. P. Cooper et al. (2023); (2) the MWBP, which is the subject of this paper; (3) the DESI Andromeda Region Kinematic (DARK) Survey (e.g., A. Dey et al. 2023); (4) standard stars observed by DESI on all dark, bright, and backup tiles; (5) the Milky Way Stream Surveys (e.g., M. Valluri et al. 2025); and (6) the Local Group Dwarf Galaxy Surveys.

The DESI Stellar Catalogs released thus far (S. E. Koposov et al. 2024; S. Koposov et al. 2026) include stellar sources observed by all of these surveys and programs, and also include any other stars serendipitously targeted by other DESI observations (e.g., as part of the DESI Main dark-time Survey or by special DESI tiles). MWS and MWBP make up the bulk of the stars in the DESI Stellar Catalog. The DARK, Milky Way Stream, and Local Group Dwarf Galaxy Surveys are targeted DESI observations made with special tiles and (so far) constitute a small fraction of the Stellar Catalog.

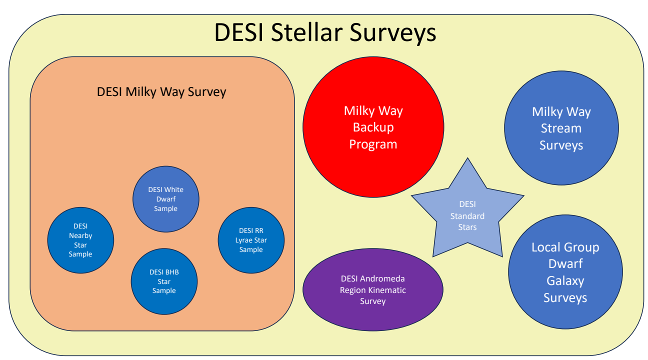

Figure 20. The current compendium and structure of the DESI Stellar Surveys. See text for details.

ORCID iDs

Arjun Dey https://orcid.org/0000-0002-4928-4003
Sergey E. Koposov https://orcid.org/0000-0003-2644-135X
Joan R. Najita https://orcid.org/0000-0002-5758-150X
Andrew P. Cooper https://orcid.org/0000-0001-8274-158X
B. T. Gänsicke https://orcid.org/0000-0002-2761-3005
A. Raichoor https://orcid.org/0000-0001-5999-7923
Daniel J. Eisenstein https://orcid.org/0000-0002-2929-3121
E. F. Schlafly https://orcid.org/0000-0002-3569-7421
D. Schlegel https://orcid.org/0000-0002-5042-5088
C. Allende Prieto https://orcid.org/0000-0002-0084-572X
Leandro Beraldo e Silva https://orcid.org/0000-0002-0740-1507
Ting S. Li https://orcid.org/0000-0002-9110-6163
M. Valluri https://orcid.org/0000-0002-6257-2341
Stéphanie Juneau https://orcid.org/0000-0002-0000-2394
Mika Lambert https://orcid.org/0000-0002-2527-8899
S. Li https://orcid.org/0000-0002-6469-8263
Guillaume F. Thomas https://orcid.org/0000-0002-2468-5521
Wenting Wang https://orcid.org/0000-0002-5762-7571
Alexander H. Riley https://orcid.org/0000-0001-5805-5766
N. Kizhuprakkat https://orcid.org/0000-0003-0853-8887
J. Aguilar https://orcid.org/0000-0003-0822-452X
S. Ahlen https://orcid.org/0000-0001-6098-7247
S. Bailey https://orcid.org/0000-0003-4162-6619
D. Bianchi https://orcid.org/0000-0001-9712-0006
D. Brooks https://orcid.org/0000-0002-8458-5047
A. Cuceu https://orcid.org/0000-0002-2169-0595
A. de la Macorra https://orcid.org/0000-0002-1769-1640
J. Della Costa https://orcid.org/0000-0003-0928-2000
Biprateep Dey https://orcid.org/0000-0002-5665-7912
P. Doel https://orcid.org/0000-0002-6397-4457
A. Font-Ribera https://orcid.org/0000-0002-3033-7312
J. E. Forero-Romero https://orcid.org/0000-0002-2890-3725
S. Gontcho A Gontcho https://orcid.org/0000-0003-3142-233X
G. Gutierrez https://orcid.org/0000-0003-0825-0517
J. Guy https://orcid.org/0000-0001-9822-6793
C. Hahn https://orcid.org/0000-0003-1197-0902
K. Honscheid https://orcid.org/0000-0002-6550-2023
M. Ishak https://orcid.org/0000-0002-6024-466X
J. Jimenez https://orcid.org/0000-0001-8528-3473
R. Kehoe https://orcid.org/0000-0002-7101-697X
D. Kirkby https://orcid.org/0000-0002-8828-5463
T. Kisner https://orcid.org/0000-0003-3510-7134
A. Kremin https://orcid.org/0000-0001-6356-7424
C. Lamman https://orcid.org/0000-0002-6731-9329
M. Landriau https://orcid.org/0000-0003-1838-8528
L. Le Guillou https://orcid.org/0000-0001-7178-8868
M. E. Levi https://orcid.org/0000-0003-1887-1018
M. Manera https://orcid.org/0000-0003-4962-8934
P. Martini https://orcid.org/0000-0002-4279-4182
A. Meisner https://orcid.org/0000-0002-1125-7384
R. Miquel https://orcid.org/0000-0002-6610-4836
J. Moustakas https://orcid.org/0000-0002-2733-4559
S. Nadathur https://orcid.org/0000-0001-9070-3102
N. Palanque-Delabrouille https://orcid.org/0000-0003-3188-784X
W. J. Percival https://orcid.org/0000-0002-0644-5727
I. Pérez-Ràfols https://orcid.org/0000-0001-6979-0125
F. Prada https://orcid.org/0000-0001-7145-8674
E. Sanchez https://orcid.org/0000-0002-9646-8198
J. Silber https://orcid.org/0000-0002-3461-0320
D. Sprayberry https://orcid.org/0000-0001-7583-6441
G. Tarlé https://orcid.org/0000-0003-1704-0781
R. H. Wechsler https://orcid.org/0000-0003-2229-011X
R. Zhou https://orcid.org/0000-0001-5381-4372
H. Zou https://orcid.org/0000-0002-6684-3997

References

Abdurro'uf, Accetta, K., Aerts, C., et al. 2022, ApJS, 259, 35
Adame, A. G., Aguilar, J., Ahlen, S., et al. 2025, JCAP, 2025, 124
Allende-Prieto, C. & Apogee Team 2023, FERRE: Match Physical Models to Measurements, Astrophysics Source Code Library, ascl:2301.016
Almeida, A., Anderson, S. F., Argudo-Fernández, M., et al. 2023, ApJS, 267, 44
Anand, A., Guy, J., Bailey, S., et al. 2024, AJ, 168, 124
Astropy Collaboration, Price-Whelan, A. M., Lim, P. L., et al. 2022, ApJ, 935, 167
Astropy Collaboration, Price-Whelan, A. M., Sipőcz, B. M., et al. 2018, AJ, 156, 123
Astropy Collaboration, Robitaille, T. P., Tollerud, E. J., et al. 2013, A&A, 558, A33
Bennett, M., & Bovy, J. 2019, MNRAS, 482, 1417
Buder, S., Kos, J., Wang, X. E., et al. 2025, PASA, 42, e051
Chiappini, C., Minchev, I., Starkenburg, E., et al. 2019, Msngr, 175, 30
Cooper, A. P., Koposov, S. E., Allende Prieto, C., et al. 2023, ApJ, 947, 37
De Silva, G. M., Freeman, K. C., Bland-Hawthorn, J., et al. 2015, MNRAS, 449, 2604
Deng, L.-C., Newberg, H. J., Liu, C., et al. 2012, RAA, 12, 735
DESI Collaboration, Abareshi, B., Aguilar, J., et al. 2022, AJ, 164, 207
DESI Collaboration, Abareshi, B., Aguilar, J., et al. 2025a, JCAP, 2025, 021
DESI Collaboration, Abareshi, B., Aguilar, J., et al. 2025b, JCAP, 2025, 028
DESI Collaboration, Abareshi, B., Aguilar, J., et al. 2024, AJ, 168, 58
DESI Collaboration, Abdul-Karim, M., Adame, A. G., et al. 2026, .AJ, 171, 285
DESI Collaboration, Abdul-Karim, M., Aguilar, J., et al. 2025c, PhRvD, 112, 083515
DESI Collaboration, Adame, A. G., Aguilar, J., et al. 2025d, JCAP, 2025, 012
DESI Collaboration, Aghamousa, A., Aguilar, J., et al. 2016, arXiv:1611.00037
Dey, A., Schlegel, D. J., Lang, D., et al. 2019, AJ, 157, 168
Dey, A., Najita, J. R., Koposov, S. E., et al. 2023, ApJ, 944, 1
Finkbeiner, D. P. 2003, ApJS, 146, 407
Gaia Collaboration, Babusiaux, C., van Leeuwen, F., et al. 2018a, A&A, 616, A10
Gaia Collaboration, Brown, A. G. A., Vallenari, A., et al. 2018b, A&A, 616, A1
Gaia Collaboration, Prusti, T., de Bruijne, J., H., J., et al. 2016, A&A, 595, A1
GRAVITY Collaboration, Abuter, R., Amorim, A., et al. 2019, A&A, 625, L10
Green, G. M., Schlafly, E., Zucker, C., Speagle, J. S., & Finkbeiner, D. 2019, ApJ, 887, 93
Guy, J., Bailey, S., Kremin, A., et al. 2023, AJ, 165, 144
Hahn, C., Wilson, M. J., Ruiz-Macias, O., et al. 2023, AJ, 165, 253
Harris, C. R., Millman, K. J., van der Walt, S. J., et al. 2020, Natur, 585, 357
Hunter, J. D. 2007, CSE, 9, 90
Jin, S., Trager, S. C., Dalton, G. B., et al. 2024, MNRAS, 530, 2688
Juneau, S., Jacques, A., Pothier,, S., et al. 2025, ASPC, 541, 77
Koposov, S. 2019, RVSpecFit: Radial Velocity and Stellar Atmospheric Parameter Fitting, Astrophysics Source Code Library, ascl:1907.013
Koposov, S., Li, T. S., Prieto, C. A., et al. 2026, OJAp, 9
Koposov, S. E., Allende Prieto, C., Cooper, A. P., et al. 2024, MNRAS, 533, 1012
Li, S., Wang, W., Koposov, S. E., et al. 2025, AJ, 170, 171
Majewski, S. R., Schiavon, R. P., Frinchaboy, P. M., et al. 2017, AJ, 154, 94
Martin, N. F., Starkenburg, E., Yuan, Z., et al. 2024, A&A, 692, A115
Miller, T. N., Doel, P., Gutierrez, G., et al. 2024, AJ, 168, 95
Myers, A. D., Moustakas, J., Bailey, S., et al. 2023, AJ, 165, 50
Poppett, C., Tyas, L., Aguilar, J., et al. 2024, AJ, 168, 245
Randich, S., Gilmore, G., Magrini, L., et al. 2022, A&A, 666, A121
Recio-Blanco, A., de Laverny, P., Palicio, P. A., et al. 2023, A&A, 674, A29
Reid, M. J., & Brunthaler, A. 2020, ApJ, 892, 39
Saydjari, A. K., Uzsoy, A. S. M., Zucker, C., Peek, J. E. G., & Finkbeiner, D. P. 2023, ApJ, 954, 141
Schlafly, E. F., & Finkbeiner, D. P. 2011, ApJ, 737, 103

Schlafly, E. F., Kirkby, D., Schlegel, D. J., et al. 2023, AJ, 166, 259
Schlegel, D. J., Finkbeiner, D. P., & Davis, M. 1998, ApJ, 500, 525
Schönrich, R., Binney, J., & Dehnen, W. 2010, MNRAS, 403, 1829
Starkenburg, E., Martin, N., Youakim, K., et al. 2017, MNRAS, 471, 2587
Steinmetz, M., Guiglion, G., McMillan, P. J., et al. 2020a, AJ, 160, 83
Steinmetz, M., Matijevič, G., Enke, H., et al. 2020b, AJ, 160, 82
Steinmetz, M., Zwitter, T., Siebert, A., et al. 2006, AJ, 132, 1645
Suda, T., Katsuta, Y., Yamada, S., et al. 2008, PASJ, 60, 1159
Suda, T., Yamada, S., Katsuta, Y., et al. 2011, MNRAS, 412, 843
Takada, M., Ellis, R. S., Chiba, M., et al. 2014, PASJ, 66, R1
Valluri, M., Fagrelius, P., Koposov, S. E., et al. 2025, ApJ, 980, 71
Virtanen, P., Gommers, R., Oliphant, T. E., et al. 2020, NatMe, 17, 261
Zhao, G., Zhao, Y.-H., Chu, Y.-Q., Jing, Y.-P., & Deng, L.-C. 2012, RAA, 12, 723
Zonca, A., Singer, L., Lenz, D., et al. 2019, JOSS, 4, 1298